DEPARTMENT OF CIVIL, GEOMATIC & ENVIRONMENT ENGINEERING

DYNAMIC BEHAVIOUR

OF

REINFORCED CONCRETE

London. 2011

Manuel Miranda

Supervisor: Dr. Paul Greening

Abstract

This work is related to the study of dynamic behaviour of civil engineering structures, using a physical experimental model.

It is aimed to associate changes in dynamic characteristics of reinforced concrete with the variation of the static load to which it is subjected.

With these objectives, it was made a reinforced concrete structure with known mechanical characteristics and it was subjected to dynamic tests for different load levels, in order to determine its modal properties – natural frequency, damping and mode shapes. At the same time, the structure was also modeled in a numerical program, which helped on the dynamic analysis.

It is expected that, after the experimental process, changes in each one of the dynamic characteristics can be correlated to the static load applied to the structure and also with its deterioration state.

List of Figures

List of Tables

List of Symbols

Section 2 - Dynamic of Structures

f_n – Natural frequency

K, k – Stiffness

M, m – Mass

C – Damping

ω – Angular frequency

ϕ – Mode shape

ξ – Modal damping factor

$H_{ij}(\omega)$ – Frequency Response Function

Section 3 – Experimental Work

ϕ – Reinforcement diameter

c – Concrete cover

F – Applied load

$f$ck – Characteristic compressive cylinder strength of concrete at 28 days

f_{ctm} – Mean value of axial tensile strength of concrete

f_y – Yield strength of reinforcement

E_c – Modulus of elasticity of concrete at 28 Days

E_s – Modulus of elasticity of reinforcement or prestressing steel

A_c – Total cross-sectional area of a concrete section

A_s – Area of reinforcement within the tension zone

d – Effective depth of a cross-section

b – Overall width of a cross-section, or actual flange width in a T or L beam

x_G – Center of gravity of a cross-section

σ_c – Compressive stress in the concrete

M_{cr} – Cracking moment

I_{ci} – Second moment of area of the homogenized section

N_{Ed} - Axial load applied

A_{ci} – Area of the homogenized section

ξ – Neutral axis depth

ρ – Reinforcement Ratio for longitudinal reinforcement

$V_{Rd,c}$ – Design value for the shear resistance

V_{Ed} - Shear load applied

Table of Contents

1. Introduction

1.1. General Considerations

The growing concerns of society with security issues have been reflected in structures engineering, in particular regarding the behavior of structures under dynamic loads. Thus, it is required, both at the project level but also at the control of already existing structures, the total knowledge of its dynamic behavior. Thus, results of the identification of its modal properties should ensure resistance, durability, safety and comfort.

Thus, it is often required a dynamic analysis in order to determine the natural frequencies, mode shapes and damping coefficient of a structure. Such analysis is usually carried out using numerical programs but also experimentally, and this last has the advantage that there are no assumptions regarding material properties, such as stiffness and damping, which occurs when modeling.

Recently, there have been important developments, both at the level of numerical modeling either at the level of technology used for the testing of vibration, which has driven the development of numerical models (e.g. Finite Elements), making them more suitable to analyze the dynamic behaviour of structures, therefore, for identification of its modal properties.

However, the reliability of numerical models can still be questioned and is not enough so they can dispense with the experimental. A structure dynamic behavior is defined by a discrete spectrum of an infinite number of natural frequencies and corresponding mode shapes, which are determinate by geometry, distribution of mass, stiffness, and boundary conditions. Reinforced concrete structures are often cracked since the moment they are erected, as the result of sudden overloading, seismic effects, corrosion, excessive temperature effects, among others. As a result, the mechanical properties of the structure are in currently change and, therefore, so is its stiffness. This way, the modal parameters change with the static load that the structure is subjected, and especially with the deteriorating state of the same.

This is where differences between experimental and numerical models occur, because the numerical programs are not yet developed to the point that such variations can be predicted in a perfect way.

This work focuses on dynamic analysis and will address, through experimental way, such variation in modal properties so as to achieve a better understanding of the phenomenon.

1.2. Motivation and Objective

In this dissertation is essentially a greater understanding about the modal properties of a reinforced concrete structure, more specifically a better understanding of how the variation of such dynamic properties is affected by the change of static loading, which is responsible for the different states of deterioration of the same.

Thus, from a simple reinforced concrete frame, it is expected to reach conclusions that might help to develop the resolution of this problem in more complex structures.

The project foresees the development of a reinforced concrete frame, all steps being addressed, i.e., since the design of the most appropriate format to the tests to ascertain its strength, so that its mechanical properties are known. Prior to dynamic testing will be carried out other tests, which arise as preparation for final testing and which include, for example, the modeling of the frame in a finite element program. With these intermediate tests it is intended a better prior knowledge of both dynamic and mechanical characteristics of the structure under study.

This way, another objective of this project is concerned with ensuring the ideal conditions for the tests in order to obtain reliable results.

For the dynamic tests carried out in the structures laboratory, they will run without any outside interference, or ensuring the minimum possible, as explained below. In addition, the structure will experience various levels of static load, to try to achieve a correlation between the loading and the variation of its modal properties.

1.3. Literature review

There are previous projects that have addressed this problem of the variation in concrete modal properties, or even another material, such as metal, due to the altered state of deterioration of the structure. In some cases, it was studied the possibility of determine damages by changing the modal parameters. Next, are presented the study's authors, as well as the most important conclusions reached. Some of them can be a starting point for the current project.

Numerous studies have indicated that increase in damage reflects decreased natural frequency of a structure. Adams et al. (1978) and Cawley and Adams (1979) developed a technique to determine the presence and location of damage in simple beams and plates using changes in modal parameters.

Initial efforts (Adams et al. 1978) focused on identifying damage in beams. The location of damage (consisting of a reduction in cross section) was accurately determined in a rectangular aluminum rod from changes in the rod's fundamental frequencies of axial vibration. Cawley and Adams (1979) recognized that the modes of vibration of a damaged beam are affected differently from the location of damage. The investigators concluded that removal of 1% of the cross-sectional area of the element could be detected using their equipment.

Chen et al. investigated the structural damage by means of the identification method of modal changes. At a critical damage level, they indicated that a decrease of the fundamental frequency up to 10% can be expected for steel beams. For reinforced concrete structures, the fundamental frequency reduction, related to the structural damage can be significantly larger. Tests showed fundamental frequency reductions of more than 60% (Pegon et al.). Such fundamental frequency decrease strongly influences the dynamic response of the structure subjected to a seismic excitation.

Brun et al. studied the change on natural frequencies of a concrete wall related with damage increase. It was carried out a finite element modeling and some tests on a real structure, so the numerical model could be validated. The experimental and numerical results indicate a reduction in frequencies with increase in damage.

Both numerical and experimental results indicated that a critical damage index has shown only less than 10% change in the frequencies of vibration. This has led to believe that the information of the natural frequency change is insufficient to be a useful indicator of structural safety. However it was also concluded that, for a severely damaged structure, the dynamic characterization method appears to be a simple technique capable of providing information about the remaining serviceability of the damaged structure. The mode shapes of the damaged structure were investigated and the results have indicated that the damage location could not be identified by the measured free-vibration mode shapes.

More recently, Horn studied in a reinforced concrete frame, subjected to the same conditions of this project, the existence of effects of application of different static loads on the change of natural frequencies and mode shapes, and that this can be seen in a rudimentary structure.

Akbarinassab et al. also developed a reinforced concrete frame in order to study the same problem, on the same test conditions. They found a decrease in natural frequencies with the increase on the static load applied, for example, the first natural frequency decreased 11% at the failure load. They also verified that the rate of change of natural frequencies was higher at the beginning of the load stages. Finally, they concluded that steel parts which they used in the frame have affected the experiment by changing the natural frequency damping the structure, and also that a more accurate method of measuring the static load than strain gages should be used.

1.4. Scope

In the Chapter 1 it is summarized the current state of the dynamic analysis of structures, covering the theoretical route and the experimental one and why it is not yet possible to use only the first one. It is described the importance of this project and the proposed targets and is still performed a bibliographic review on the subject to study.

In the Chapter 2 are presented the theoretical principles which will underpin the project, covering an introduction to the modal analysis and to some modal testing techniques.

The Chapter 3 is entirely reserved for experimental process. It is described all steps of testing and dynamic analysis, but also other tests in preparation for that analysis. At the beginning of the chapter, for example, it is described the whole conception of the frame under study.

In the Chapter 4 are presented the results of all tests as well as the discussion of them.

In Chapter 5 are presented the conclusions of this research. There are also some recommendations for further work and possible criticisms to this project.

2. Dynamic of Structures

2.1. Modal Analysis and Structural Models Behaviour

The introduction of this theme aims at addressing some of the fundamentals of the dynamic of structures, which are associated to the study of the response of models.

The data acquisition about the response and its subsequent analysis, under closely controlled conditions, where a structure is vibrated with a known excitation is called Modal Testing.

However, first it will be addressed the theme of modal analysis in a more embracing way.

As already mentioned, a structure dynamic behaviour is defined by a discrete spectrum of an infinite number of natural frequencies and corresponding mode shapes. The modal analysis is the process consisting of experimental and theoretical techniques that allow the construction of a mathematical model of the system under study, in order to determine its modal parameters – natural frequencies, mode shapes and damping factors.

Natural frequencies indicate the rate of free oscillation of a structure, after ceasing the force that led to its movement. In similar words, is how much a structure vibrates when there is no force applied on it. This frequency is a direct function of stiffness, and an inverse function of the mass of the structure. A structure has several natural frequencies because it can vibrate freely (after excited by a force) in several directions.

$$f_n = \frac{1}{2\pi}\sqrt{\frac{k}{m}}$$

Mode shapes are the way a structure vibrates. Each one is related to its natural frequency, i.e., for each natural frequency there is a specific way of vibration. Damping is an internal property of dissipating energy, which tends to reduce the amplitude of oscillations leading to the end of the oscillatory movement.

Such parameters are often determined by analytical methods (e.g. Finite Element program), however, there are situations where the analytical model does not exist, so the modal parameters can be determined experimentally. Sometimes, even if it exists, the experimental approach can be used for verification and validation of the analytical model.

Thus, there are two different routes to vibration analysis, in order to obtain dynamic properties, the theoretical and the experimental, which will be addressed then.

2.1.1. Theoretical Route

The theoretical route starts with a description of the structure's physical properties, by defining its mass matrix (M), damping (C) and stiffness (K), which is referred as the Spatial Model.
Subsequently, it is made a theoretical modal analysis of the spatial model, determining the so-called Modal Model: a set of natural frequencies (ω), with corresponding mode shapes (ϕ) and modal damping factors (ξ). This solution always describes the various ways in which the structure is capable of vibrating without external forcing or excitation.

The last phase, which will give us the Response Model, is that where the response of structure under the influence of an excitement is analyzed. This will depend not only upon the structure's properties but also on the nature and magnitude of the excitation. Thus, it is convenient to present this analysis to a standard excitation. From this standard excitation, the solution of any particular case may be built. The Response Model consists of a set of Frequency Response Functions (FRFs).

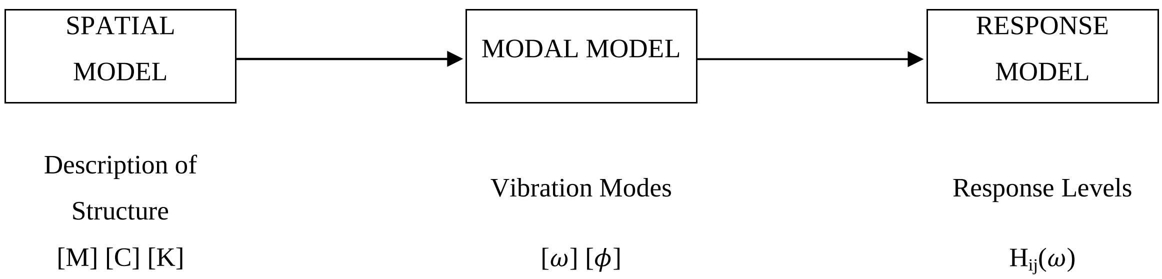

Figure 2.1 – Theoretical Route to Vibration Analysis

2.1.2. Experimental Route

The experimental route to vibration analysis is called Modal Testing, and this is the route addressed in this project. As mentioned before, it is the process involved in testing structures with the objective of obtaining a mathematical description of their dynamic or vibration behaviour.

This route starts by testing a structure on a laboratory. There is measured its response to a known excitation and that data is analyzed by a software. Modal parameters are determined from the construction of FRF's, which relate the excitation with the response of the structure. Because it is a complex quantity, the frequency response function cannot be fully displayed on a single two dimensional plot. It can, however, be presented in several formats, each of which has its own uses, and some of them will be discussed later.

It is generally accepted that corroboration of the major modes of vibration by tests can provide reassurance of the basic validity of the theoretical model. Thus, both methods, theoretical and experimental must be used in modal analysis – the experimental to validate the experimental model, and the theoretical to analyze structures too complex to be simulated in a laboratory.

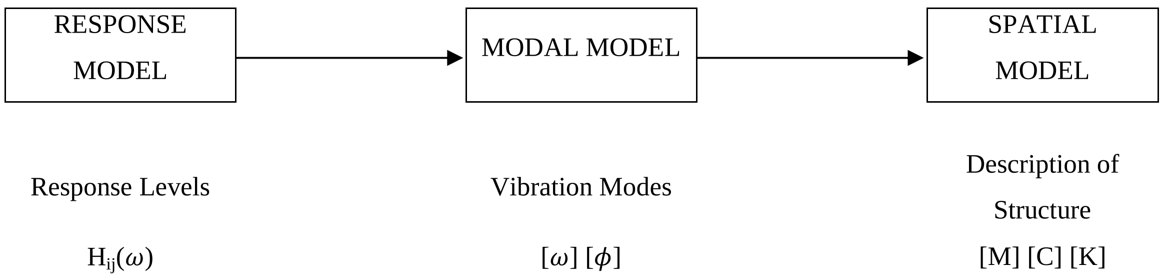

Figure 2.2 – Experimental Route to Vibration Analysis

Back to the experimental route of vibration analysis, the type of test best suited to FRF measurement is the one with a single-point excitation, which requires attention in the some points that will be reviewed in the next section, they being the mechanical aspects of supporting, the excitation of the structure and the correct transduction of the quantities to be measured.

2.2. Modal Analysis Techniques

As it was mentioned in the previous section, here it will be discussed some questions about the FRF measurement system, such as how the structure should be suspended or supported, how it should be excited and how the parameters – input force and structure response – needed to the FRF's construction should be measured. At the end of this section will be presented measurement improve techniques as well as some FRF formats. All this section is based on *Modal Testing,* from Ewins, 2000.

2.2.1. Structure Supporting

The supports can be in form of either free supports, suspended on soft springs, grounded supports, with rigid supports at certain points and in-situ where the object is attached to a non-rigid attachment structure. In the FE analysis software, free supports are easier to model and hence it is usual to choose this type of support on the experimental model. This type of support mainly relies on the basis that the structure is not connected to ground at any of its nodes, in other words it is freely suspended in space. This situation allows a more accuracy study on the modal properties of a structure, without external interference that could change some of those properties. In practice it clearly is not possible to have prefect free support for any structure, therefore this problem is tackled by providing very soft springs. It has been proved that the spring does not have minimal effects on the modes of vibration and natural frequencies of the structure, as the rigid body modes are significantly less than the bending modes, and hence can be reliable to proceed.

Figure 2.3 – Free Support

2.2.2. Excitation of the Structure

There are several ways to carry out the excitation tests on the object. It can be done with a contacting or a non-contacting method, which means that the exciter can remain attached to the structure or not. There are advantages and disadvantages associated with these methods but the choice of excitation is more based on the type of analysis done and the range of frequency that the structure is to be vibrated. The most common ways for each one of these methods are the shaker and the impact hammer, respectively.

The Impact Hammer is categorized as a transient force and it is the one that it will be used in this experimental work.

An ideal impact to a structure is a perfect impulse, which has an infinitely small duration, causing a constant amplitude in the frequency domain. This would result in all modes of vibration being excited with equal energy. The impact hammer test is designed to replicate this. However, in reality a hammer strike cannot last for an infinitely small duration, but has a known contact time. The duration of the contact time directly influences the frequency content of the force, with a larger contact time causing a smaller range of bandwidth. A load cell is attached to the end of the hammer to record the force. Impact hammer testing is ideal for small light weight structures.

Figure 2.4 – Impact Hammers

2.2.3. Data Acquisition

The piezoelectric type of transducer is the most widely used for sensing force and motion in modal testing. The mechanism of the force transducer is called load cell and, as it was mentioned before, is attached to the exciter.

The mechanism of the response transducer is called accelerometer. The correct location of accelerometers is most important because they should not be positioned at or very close to a node of one or more of the structure's modes. Thus, most modal tests require a point mobility measurement. In order to measure a true point FRF both force and response transducers should be at the same point on the structure, which can be achieved by placing them in line but on opposite sides of the frame.

The data acquired is then processed and exported to a computer by a specific device.

Figure 2.5 – Accelerometer

2.2.4. Improving Measurement Accuracy

There are several techniques that can be used in order to improve the acquired data.

In order to reduce the statistical variance of a measurement with a random excitation function (such as random noise) and also reduce the effects of nonlinearities, it is necessary to employ an averaging process. By averaging several time records together, statistical reliability can be increased and random noise associated with nonlinearities can be reduced.

It can be used a low-pass filter, which is an electronic device that has a circuit inside which gives easy passage to low frequencies and difficult passage to high frequencies.

Another measurement capability that is often needed is to obtain more frequency resolution. The capability to zoom allows closely spaced modes to be more accurately identified.

Figure 2.6 – Low-Pass Filter

2.2.5. FRF Presentation

A frequency response function (FRF) graphic is going to be very useful in this project. Through that, it is possible to identify natural frequencies of a system.

Because it is a complex quantity, the frequency response function cannot be fully displayed on a single two dimensional plot. It can, however, be presented in several formats, each of which has its own uses.

The following types of plots are mainly used to present FRF data.

The Bode plot consists of two plots, one amplitude (modulus of FRF) vs. frequency and the other phase vs. frequency. The problem with the linear scale FRF is the wide variation of the values that must be considered. Therefore the log scale is used here instead of the linear scale.

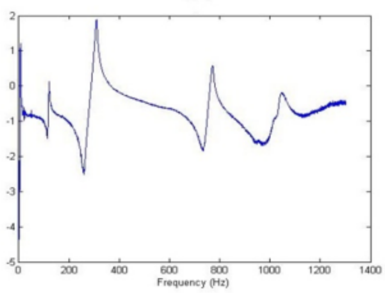

Figure 2.7 – Bode Plot

Each one of the peaks seen in the Figure 2.7 is a natural frequency.

Resolving the phase portion into two orthogonal components is another way of presenting FRF data: one in-phase part (real part), and one part 90 degrees out of phase (imaginary part). For this form of presentation, the use of log scale is not beneficial since it is essential to contain both positive and negative values and this would not be possible with the log scale.

When the above phase parts are plotted against each other, the data representation is called the Nyquist plot.

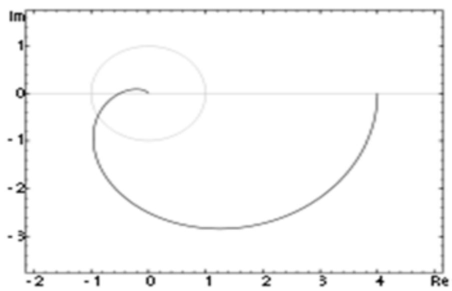

Figure 2.8 – Nyquist Plot

3. Experimental Work

3.1. Frame Design

3.1.1. Final Solution

As already mentioned, with the aim of studying the change of the dynamic properties according to the variation of the static load applied, it was developed a reinforced concrete structure, knowing beforehand that this would have to be subject to some test conditions. Thus, it should be a simple frame, not too heavy, which permitted its suspension with soft springs. In addition, the static load should be applied easily and without implying that the same had any contact with an external element. Finally, the load should be applied so as to confer flexion.

As it was said before, steel parts can modify structure modal properties, so it was only used steel on the reinforcement.

Figures 3.1 and 3.2 present the chosen solution, with detailed dimensions. Note that the dimensions were determined on the assumption that the frame would have a final weight of approximately *15 Kg* and that the reinforced concrete had a volume weight of *25 Kg/m*^{3}.

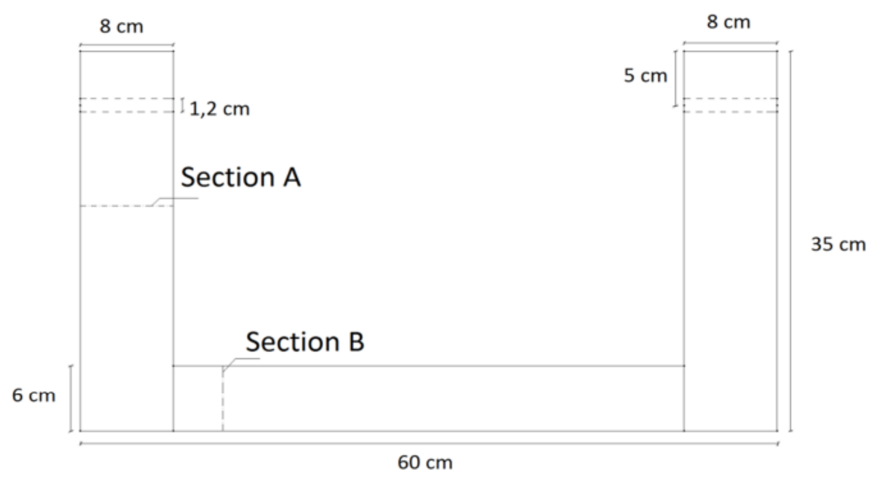

Figure 3.1 – Concrete Frame Solution

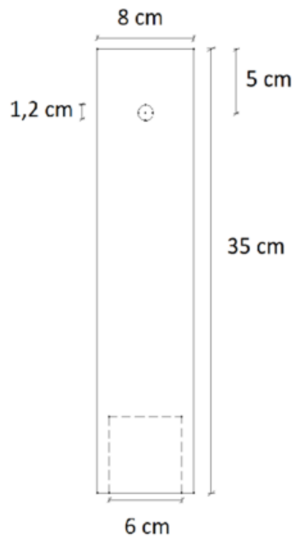

Figure 3.2 – Side View of the Concrete Frame Solution

The frame consists of an 'U' structure. There are two different sections, the section A on the side beams and the section B on the middle section. Both are presented on Figures 3.3 and 3.4.

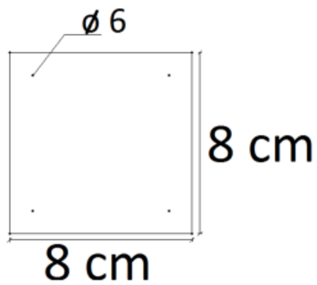

Figure 3.3 – Section A

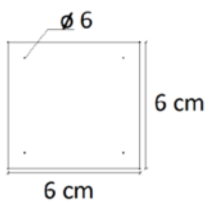

Figure 3.4 – Section B

The middle section – section B – is smaller, so as to ensure that is there where the major structural damage will occur, since this is the area to study. One of the main considerations in the design of the frame was to make sure that is this section that fails under loading. In addition, it was sought to have the failure occurring away from the loading points.
There will be a *10 mm* steel bar through the two holes on the side beams. The purpose of the steel bar is to be the mechanism of strength application, operating simply by tightening the bolts on both ends. As the load is exerted to the side beams, there will be an axial compression force and a bending moment applied to the concrete section where the failure in the frame will occur. Moreover, this steel bar will be fitted with a load cell which will assist in identifying the load applied to the frame. Making sure that the maximum stress applied to the bar does not exceed its yield stress, each load can be matched to each strain applied on the load cell. Therefore, the strain readings during the experiment can indicate the loads applied to the frame. The hole dimensions are explained on the section 3.1.3.
Figures 3.5, 3.6, 3.7, 3.8 and 3.9 show the detail of the reinforcement. It was chosen for the whole reinforcement a *6 mm* diameter and a concrete cover of *1 cm*.

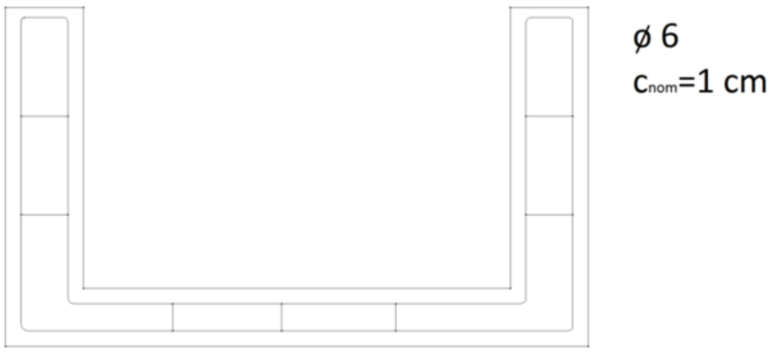

Figure 3.5 – Frame Reinforcement

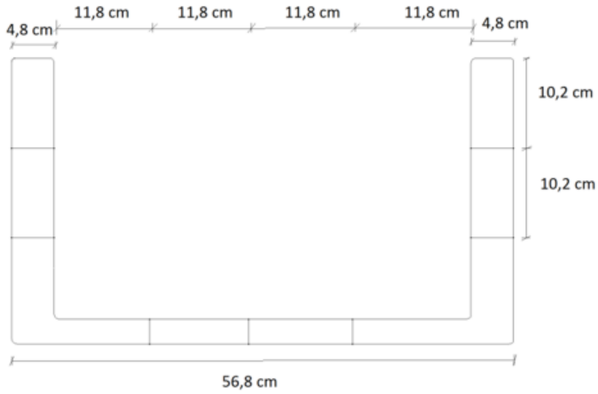

Figure 3.6 – Reinforcement Details

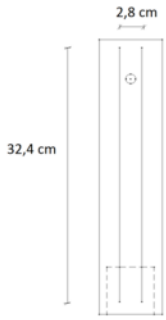

Figure 3.7 – Side View of the Reinforcement

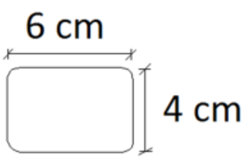

Figure 3.8 – Section A Reinforcement

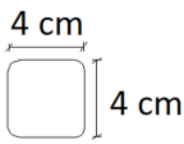

Figure 3.9 – Section B Reinforcement

3.1.2. Design of Steel and Concrete Sections

Chosen the reinforced concrete frame, then it were calculated the total strength expected to apply until the crack and until the rupture of Section B.

Figure 3.10 shows the frame scheme from which the shear, bending moment and tension diagrams were made. These diagrams can be seen in figures 3.11, 3.12 and 3.13.

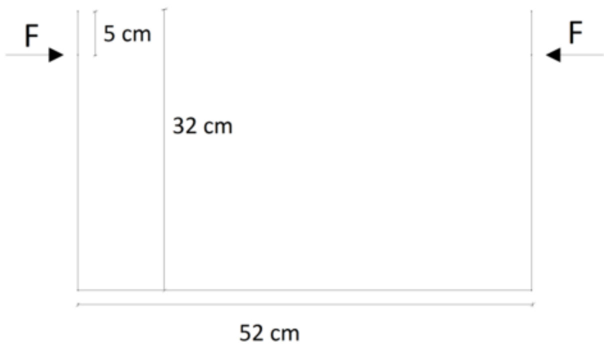

Figure 3.10 – Frame Scheme

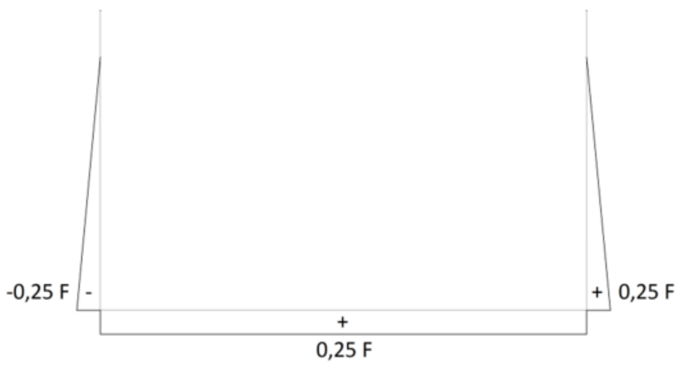

Figure 3.11 – Bending Moment Diagram

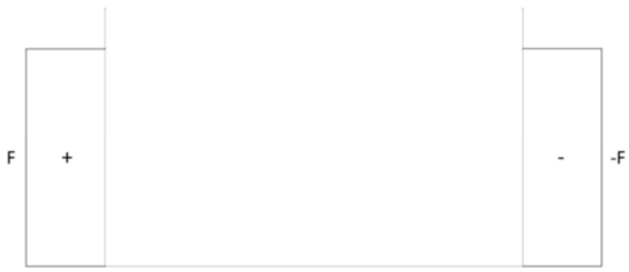

Figure 3.12 – Shear Force Diagram

Figure 3.13 – Axial Load Diagram

Note that the values used in the calculations for the strength of steel are the result of tensile test, presented in *Appendix 1*, and it was admitted that the concrete was the C35/45, which was the chosen concrete type to use on the frame.
It was also made the shear verification in Section A. All the calculus can be seen in next sections.

In table 3.1 can be seen some concrete frame properties and some values from *Eurocode 2 – Design of Concrete Structures* – required to the referred calculations.

Table 3.1 – Concrete Frame Properties

Concrete Frame Properties		
f_{ck} *(MPa)*	*35*	
f_{ctm} *(MPa)*	*3,2*	
f_{yk}*(MPa)*	*375*	
E_c *(GPa)*	*34*	
E_s *(GPa)*	*200*	
A_c (m^2)	*Section A – 0,0064*	*Section B – 0,0036*
A_s $(m^{2)}$	*Section A –* $1{,}131x10^{-4}$	*Section B –* $1{,}131x10^{-4}$
d (m)	*Section A – 0,067*	*Section B – 0,047*
b (m)	*Section A – 0,08*	*Section B – 0,06*
c (m)	*0,01*	
ϕ *(m)*	*0,006*	
x_G *(m)*	*Section A – 0,04*	*Section B – 0,03*

3.1.2.1. Cracking Moment – *Section B*

$$\sigma_c = f_{ctm}$$

$$\frac{M_{cr}}{I_{ci}} y_{inf} - \frac{N_{Ed}}{A_{ci}} = 3{,}2$$

where,

$$y_{inf} = 0{,}03\ m$$

It is known, by observing figures *3.11*, *3.12* and *3.13*, that:

$$M_{cr} = 0{,}27F$$

$$N_{Ed} = F$$

As the section is composed by two different materials – steel and concrete – it is required the homogenization in one of them in order to determine the area and second moment of area of the section.

It was admitted a homogenization in concrete:

$$\alpha = \frac{E_s}{E_c} = \frac{200}{34} = 5{,}88$$

So, the second moment of area of the homogenized section and its area are the following:

$$I_{ci} = \frac{b^4}{12} + \frac{A_s}{2}\alpha(d - x_G)^2 + \frac{A_s}{2}\alpha(x_G - c - \frac{\phi}{2})^2$$

$$I_{ci} = 1{,}272 \times 10^{-6}\ m^4$$

$$A_{ci} = A_c + (\alpha - 1)A_s$$

$$A_{ci} = 41{,}52\ \ cm^2$$

So, the load and the corresponding cracking moment are:

$$F = 0{,}52\ KN$$

$$M_{cr} = 0{,}14\ KN \cdot m$$

3.1.2.2. Ultimate Moment – *Section B*

In order to determine the ultimate moment and the corresponding static load, it were used the following expressions, which derive from others from the *Eurocode 2*.

$$\sigma_c = C_c \frac{M_s}{bd^2} = f_{ck} = 35\ MPa$$

$$\sigma_s = C_s \frac{M_s}{bd^2} = f_{yk} = 375\ MPa$$

On the first one, the structure fails due to crushing of concrete, while in the second one is reached the flexural tensile strength of reinforcement. It will be calculated the load for both situations and the smaller is, obviously, the cause of failure in this frame.

Firstly, it will be determined the load that will crush the concrete:

$$C_c = \frac{\xi}{\frac{\xi}{2}\left(1 - \frac{\xi}{3}\right) + \rho' \alpha \left(1 - \frac{d'}{d}\right)(\xi - \frac{d'}{d})}$$

$$\xi^3 - 3\left(1 + \frac{e}{d}\right)\xi^2 + 6\alpha\rho\left[-\frac{e}{d} + \frac{\rho'}{\rho}(-\frac{e}{d} - 1 + \frac{d'}{d})\right]\xi - 6\alpha\rho\left[-\frac{e}{d} + \frac{\rho'}{\rho}(-\frac{e}{d} - 1 + \frac{d'}{d})\right] = 0$$

$$e = \frac{M_s}{N} = \frac{M}{N} + e_s = \frac{0{,}27F}{-F} + e_s = -0{,}27 + e_s$$

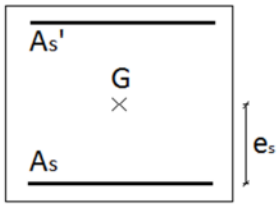

Figure 3.14 – Reinforcement Eccentricity

$$e_s = 0{,}017\ m$$

$$e = -0{,}253\ m$$

$$M_s = 0{,}253F$$

$$\alpha = \frac{E_s}{E_c} = 5{,}88$$

$$\rho = \frac{A_s}{bd} = 0{,}02005$$

$$\rho' = \frac{A_s'}{bd} = 0{,}02005$$

$$\xi = 0{,}506618\ m$$

$$C_c = 4{,}012$$

$$M_s = 1{,}16\ KN \cdot m \rightarrow F = 4{,}57\ KN$$

Next, it is presented the determination of the load that would be responsible to the frame failure due to tensile on reinforcement.

$$C_s = \alpha \frac{1-\xi}{\xi} C_c$$

$$C_s = 22{,}974$$

$$M_s = 2{,}16\ KN \cdot m \rightarrow F = 8{,}54\ KN$$

So, it is expected that the frame fails due to crushing of the concrete on section B, when a load of, approximately, *4,5 KN* is reached.

3.1.2.3. Shear Verification – Section A

According to *Eurocode 2*:

$$V_{rd,c} = C_{rd,c} \times k \times (100 \times \rho_l \times f_{ck})^{1/3} \times b \times d > V_{Ed}$$

where,

$$C_{rd,c} = 0{,}12$$

$$\rho_l = \frac{A_{sl}}{b \times d} = 0{,}0275$$

$$k = 1 + \sqrt{\frac{200}{d}} = 2{,}777$$

So,

$$V_{rd,c} = 7{,}8\,KN > V_{Ed} = F = 4{,}57\,KN$$

It is verified that the side beams will resist without any problem to shear force.

3.1.3. Determination of the Hole Dimensions – Section A

In previous works – Horne and Akbarinassab – it was found that when applying the load, as the frame is deformed, the steel bar came in contact with the structure in the holes of the side beams, as shown in Figure 3.15.

Figure 3.15 – Steel Bar in Contact with Concrete

That eventually changed some dynamic properties.

To try to prevent this phenomenon from happening, it was tried to calculate the diameter needed for the hole in section A in order to, when the maximum deflection happens, avoid the contact between the bar and the structure. Then are presented the calculations and in *Appendix2* are shown the figures obtained in software *Ftoll*, where the displacements were calculated corresponding to the maximum load to be applied, which was calculated in previous section – *4,5 KN*.

The maximum horizontal displacement, from the software *Ftoll*, is *2,3 mm.* However, it was admitted a value of *5mm*, for safety.

The Figure 3.16 shows the scheme that allowed the determination of the hole diameter. Those calculations are presented next.

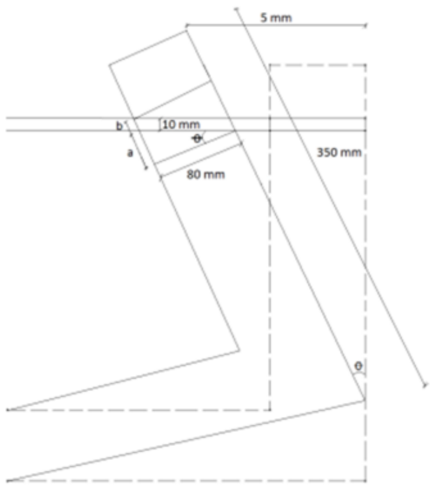

Figure 3.16 – Hole Diameter

$$\sin(\theta) = \frac{5}{350} \Rightarrow \theta = 0{,}818^{o}$$

$$tg(\theta) = \frac{a}{80} \Rightarrow a = 1{,}143\ mm$$

$$\cos(\theta) = \frac{10}{b} \Rightarrow \mathrm{b} = 10{,}001\ mm$$

$$\mathrm{a} + \mathrm{b} = 11{,}144\ mm$$

So that is the minimum value for the hole diameter. It was decided that it should be *12 mm*.

3.1.4. Frame Construction and Crack Zone Study

With all the dimensions of the structure determined, it was carried out the concreting of four identical frames in the laboratory, along with a few cubes to demonstrate the strength of concrete used. It was decided concreting four frames not only to compare the results of dynamic tests and thus reinforce the conclusions reached, but also to prevent any mistakes or lack of effective method applied in these dynamic tests.

Figures 3.17 to 3.20 show the concreting process.

Figure 3.17 – Frame Mold

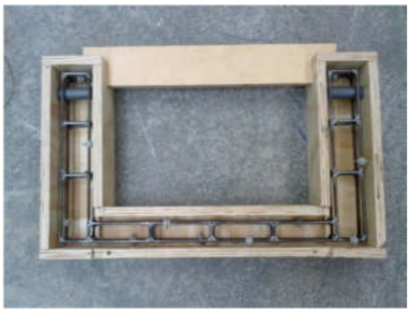

Figure 3.18 – Frame Mold with the Reinforcement

Figure 3.19 – Concrete

Figure 3.20 – Frames and Cubes after Concreting

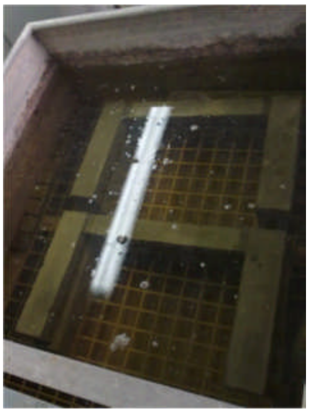

Figure 3.21 – Curing of Concrete

Frames were numbered from one to four.

Note that, possibly due to a large amount of water in the concrete, it were verified some deformations on some areas of the frames, as it can be seen in Figures 3.22 and 3.23, where are shown some of the referred deformations.

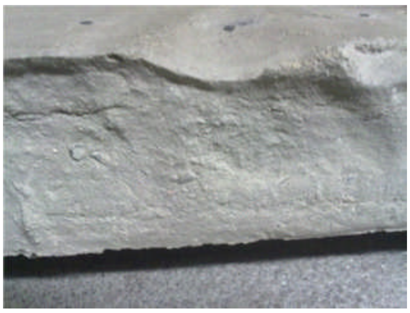

Figure 3.22 – Deformations on Concrete Frame

Figure 3.23 – Deformation on Concrete Frame

During this process it was also the concreted a beam, whose dimensions and armor are presented in figures 3.24 to 3.26.

Figure 3.24 – Beam Dimensions

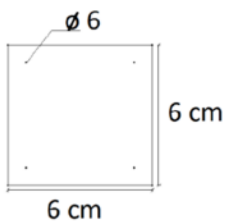

Figure 3.25 – Beam Section

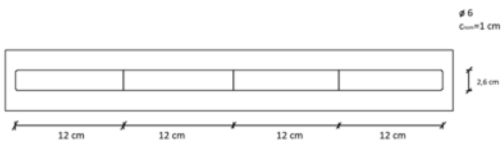

Figure 3.26 – Beam Reinforcement

The aim would be to obtain a structure with mechanical properties similar to those of section B of the frame where the dynamic tests will occur.

Figure 3.27 – Beam Mold

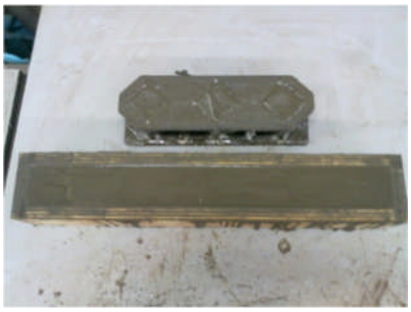

Figure 3.28 – Beam after Casting

Thus, this beam was tested until failure to determine its ultimate moment, in order to confirm the calculations made for the frame. Beyond that, this beam was built to check its failure area.

The detailed calculations of the ultimate moment of the beam are shown on *Appendix 3* and on *Appendix 4* it is presented the compression test carried out on cubes that were concreted together, in order to confirm that the concrete strength is *35 MPa*, as it was expected.

The final results of both tests are presented next.

$$\sigma_c = 34{,}4\ MPa$$

This is almost the same as the expected strength.

$$M = 1{,}21\ KN \cdot m$$

By observing the figure 3.11, which is referred to the bending moment diagram of the structure that will be studied on dynamic tests, its moment in section B is:

$$M = 0{,}27\ F$$

It means that, if that middle beam of the frame behaves in a similar way of this beam, it will fail when the static load applied is:

$$F = \frac{1{,}21}{0{,}27} = 4{,}48\ KN$$

It should be mentioned that this is a very similar value to the one which was predicted on calculations on section 3.1.2.2.

As it was expected, from the calculations on section 3.1.2.2, the beam failed due to crushing of the concrete.

3.1.5. Finite Element Modelling

Before the dynamic tests were carried out, the structure was modeled on the software *GSA*, in order to determine its natural frequencies so that, when the final tests start, these were previously known.

There were defined the concrete and steel sections so that the model could present a similar behaviour to the real structure. The model consists of a total of twenty four elements, which include two different sections of concrete, the steel bar and five springs. The four springs introduced at the ends of the frame intended to simulate the condition of free support, and the one introduced in the middle of the center beam is rotational.

All movements were prevented in the z direction, including the rotations *xx* and *yy*.

The model is represented in figure 3.29.

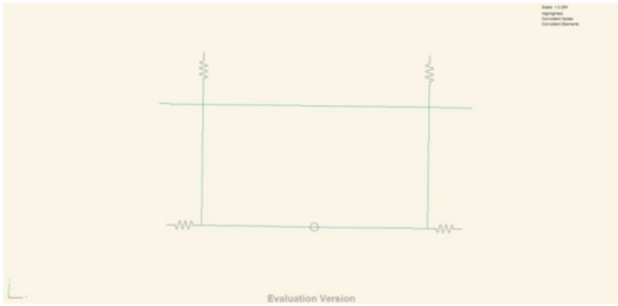

Figure 3.29 – GSA Model

A dynamic analysis was carried out and the natural frequencies obtained are presented next. It must be mentioned that the frequencies above *1000 Hz* were filtered. Corresponding mode shapes are represented in figures 3.30 and 3.31.

$$f_1 = 155{,}2\ Hz$$

$$f_2 = 643{,}3\ Hz$$

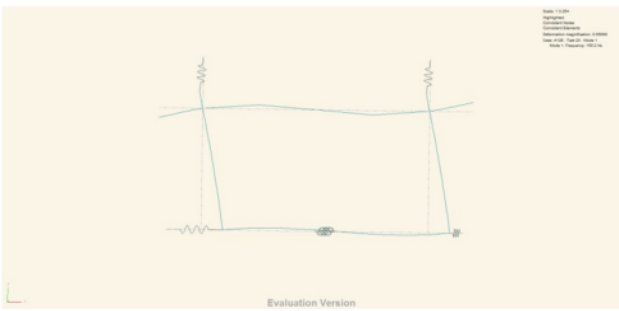

Figure 3.30 – First Mode Shape

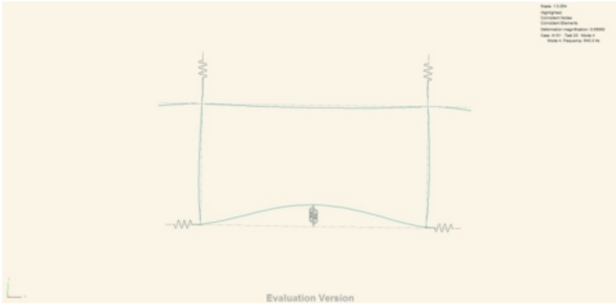

Figure 3.31 – Second Mode Shape

The structure was also modeled without the steel bar and it was obtained an extra natural frequency below the *1000 HZ.* The natural frequencies obtained were the follow:

$$f_1 = 129{,}4\ Hz$$

$$f_2 = 315{,}1\ Hz$$

$$f_3 = 786{,}4\ Hz$$

3.1.6. Load Cell Calibration and Load Steps Definition

As already mentioned, the determination of the static load applied will be done by using a load cell. This is provided with strain gages and, using a strain indicator where the load cell is connected extensions corresponding to each load will be read. Figure 3.32 shows a strain indicator.

Figure 3.32 – Strain Indicator

For this, it was needed a calibration test in which the load cell was loaded with weights until *20 Kg* in increments of *1Kg*, unloaded and then loaded again until *20 Kg* in increments of *2Kg* and finally in increments of *5Kg*. In figure 3.33 it is represented this test.

Figure 3.33 – Load Cell Calibration

Strain was measured to each load level, allowing the construction of the graphic *Load vs strain.* All the results, including this last graphic are presented in *Appendix 5*. In Figure 3.34 is shown the referred graphic.

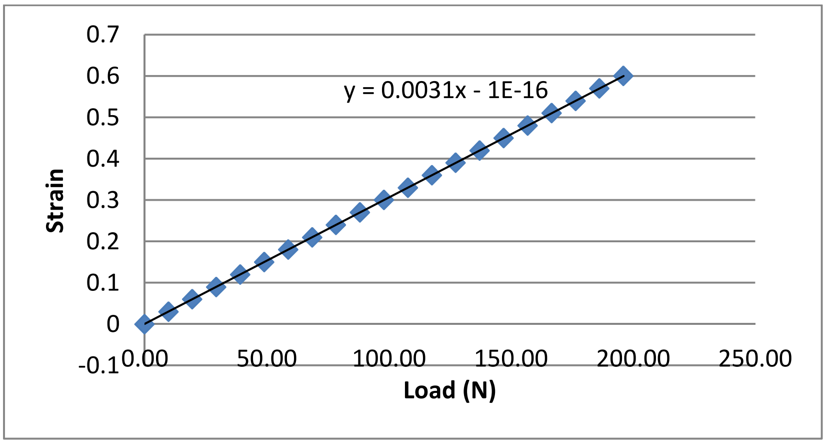

Figure 3.34 – Graph of Load vs Strain

Knowing the equation of the last graphic and also the loads which correspond to cracking and ultimate moment, it were chosen the load levels for the dynamic tests. In table 3.2 are presented these values as well as the corresponding strains.

Table 3.2 – Load Levels Definition and Corresponding Strains

Load (N)	*Strain*
0	0
125	0,375
250	0,75
375	1,125
500	1,5
625	1,875
750	2,25
875	2,625
1000	3
1125	3,375
1250	3,75

Load (N)	*Strain*
1375	4,125
1500	4,5
1625	4,875
1750	5,25
1875	5,625
2000	6
2125	6,375
2250	6,75
2375	7,125
2500	7,5
2625	7,875

Load (N)	*Strain*
2750	8,25
2875	8,625
3000	9
3125	9,375
3250	9,75
3375	10,125
3500	10,5
3625	10,875
3750	11,25
3875	11,625
4000	12

3.2. Dynamic Tests

In this section it will be addressed the dynamic tests performed. In the first place, support conditions and excitation of the structure will be described, and then it will be presented the methods and materials.

It should be mentioned that, the methodology described in this section will be carried out not only to study the change the of dynamic characteristics due to application of static load, which is the main objective of this research, but it will also be used in other intermediate tests, such as the variation of the natural frequencies over time and others aimed at improving the quality of data.

3.2.1. Test Conditions

For reasons stated above, it was decided to suspend the structure from the ceiling by springs in order to simulate the free support condition, as it can be seen in Figure 3.35.

Figure 3.35 – Simulation of the Free Support

It should be noted that an optimum position for the spring was chosen in order to balance the structure while it is suspended.

As far as the excitation is concerned, this will be done by using an impact hammer, whose characteristics have been presented above.

3.2.2. Hammer Impact Test

With the structure suspended, its response data were acquired using an accelerometer placed at different points, as will be mentioned below, and a force transducer attached to the impact hammer that provides data on the force imposed on the frame.

Both devices referred above are connected to a power amplifier, which controls the magnitude of the signal, which is then filtered by a low-pass filter. The range for this filter will also be discussed below.

Figure 3.36 – Power Amplifier

Finally the signals are routed to the Picocope and then to the computer where, using the software developed by Paul Greening *Abets* in *Matlab*, data will be analyzed.

Figure 3.37 - Picoscope

As already mentioned, the load cell and the strain indicator allow the application of the required load. That is done by tightening the nuts on the ends of the bar until it is reached the strain corresponding to each load level. The process of introducing the load is shown Figures 3.38, 3.39 and 3.40.

Figure 3.38 – Load Cell Placed in the Middle of the Bar

Figure 3.39 – Application of the Load

Figure 3.40 – Strain Indicator Registering Strain Values from Load Cell

In the following figure is schematized the all process.

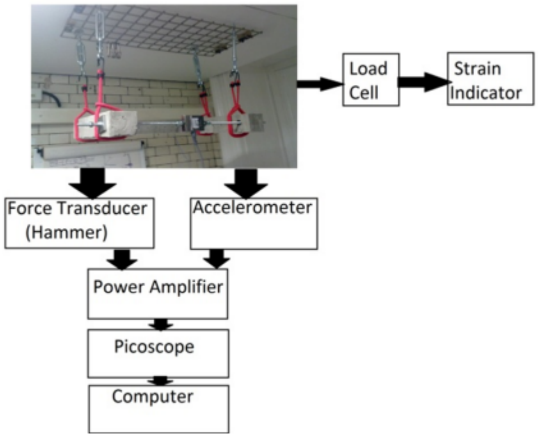

Figure 3.41 – Scheme of the Process

3.2.2.1. Intermediate Tests

Prior to the final tests, others were carried out in the frame 2 in order to improve the quality of data acquired, which included determining the sample rate of frequencies to study and also the number of hammer hits to made in each measurement.

On the study of the sample rate, software *Abets* provides different possibilities. Measurements were made according to the procedure described above, and taking into account the values of frequencies obtained on the *GSA* model.

It should be noted that the low-pass filter is directly related to the sample rate of frequencies and it has a value of 0,4 times the range.

In Figure 3.42 is presented the sample rate that was decided to study.

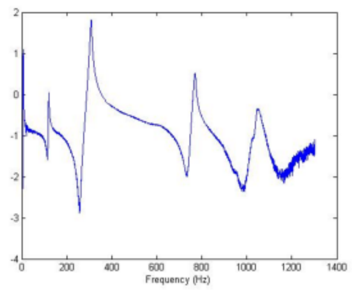

Figure 3.42 – Sample Rate under Study

That sample rate requires a filter of *1000 Hz*, which means that all values above should be ignored. In Figure 3.43 it is shown that the peak on *1100 Hz* from figure 3.42 it is not a natural frequency.

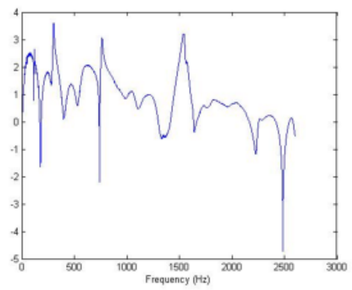

Figure 3.43 – Measurement with a higher Sample Rate

Finally, measurements were made with *6*, *8* and *10* hits, and then it was made the average of the obtained data. That can be seen in Figure 3.44.

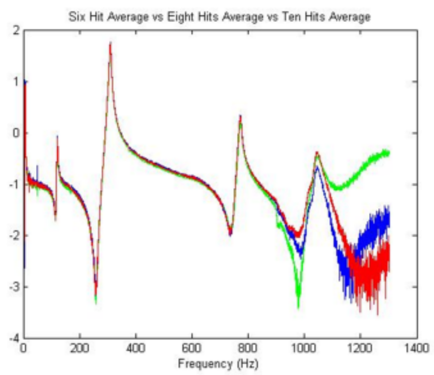

Figure 3.44 – Measurement with 6 (green), 8 (blue) and 10 (red) hits

It was concluded that the measurements with *10* hits had sufficient quality, so this will be the number of hits to make in the final dynamic tests.

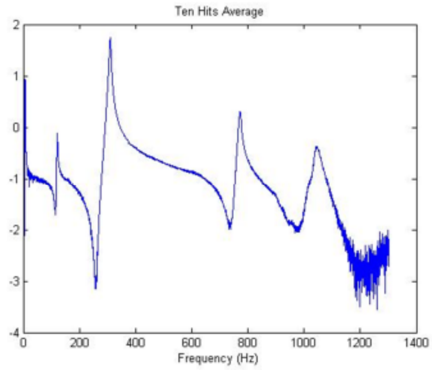

Figure 3.45 – Measurement with 10 hits

Thus, from now on, all the measurements are referred to an average of *10* hammer hits.

3.2.2.2. Final Tests

3.2.2.2.1. Frequency vs Time

It was carried out another test where the structure was not loaded. *Frame 2* was tested for nine days, collecting FRF's in each one of those days. The aim was to study the change on natural frequencies over time. Note that the start of these tests took place *28* days after casting.

The structure was tested in accordance with the procedure described above, with the accelerometer and impact area with the hammer constant.

Since the determination of the load would not be necessary, the frame was tested without the steel bar.

Results and their discussion are presented in section 4.

3.2.2.2.2. Modal Carachteristics vs Load

The main case of study of this research was analyzed according to the procedure described in section 3.2.2., and, for that, were initially defined the locations of the accelerometer and the excitation area. All frames were marked with a set of *16* points and the position of those points is shown in Figure 3.46.

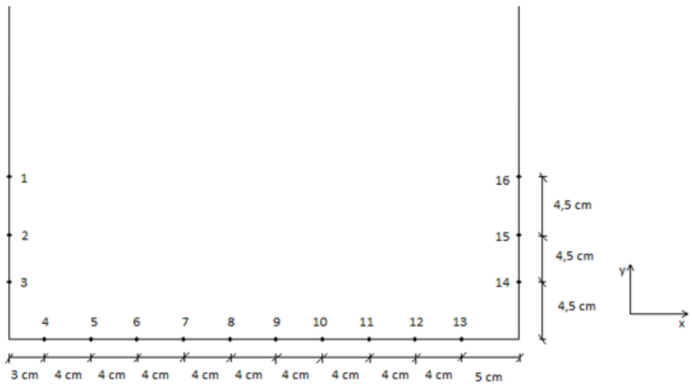

Figure 3.46 – Points Tested

The accelerometer remained throughout the test in point *5*, collecting the response data in *direction y.*

The excitation was carried out on the opposite side of the frame, also in *direction y.* The hammer hits were taken at different points for each load level. Points where the excitation was carried out for each load level are shown in Table 3.3.

Table 3.3 – Excitation Points

Load Level (N)	***Excitation point***
0, 1000, 4000	All points were tested
500, 1500, 2000, 2500, 3000, 3500	5, 7, 9, 11, 13
All other load levels	5

This was decided so that, for some load levels, was possible the representation of mode shapes of the structure.

De notar que foram ainda registados o número de voltas a aplicar na porca para atingir cada carga.

To obtain values of damping and mode shapes, was used the software *Icats* which determined these modal characteristics from FRF's obtained before.

This test was carried out on frames *1 and 3.*

Results are presented in section 4, along with its analysis.

4. Results

4.1. Frequency *vs* Time

Following plots show changes in natural frequencies of the structure in just *9* days. As it was expected from the *GSA* analysis, were identified three natural frequencies, each one of them corresponding to the peaks seen in next figures.

Figure 4.1 presents FRF's overlaid for the first and seventh day in order to demonstrate possible changes in the first week.

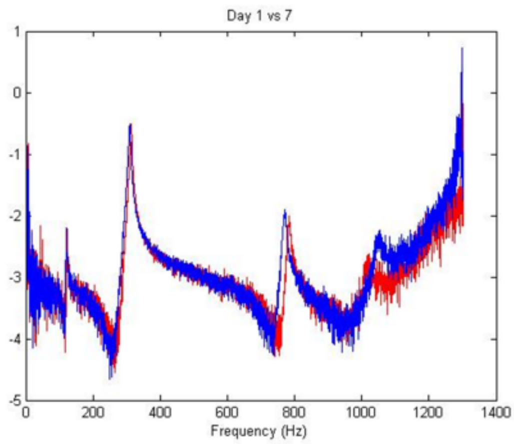

Figure 4.1 – FRF's from the 1st and 7th day

Figure 4.2 shows FRF's overlaid from the first and last day of this test.

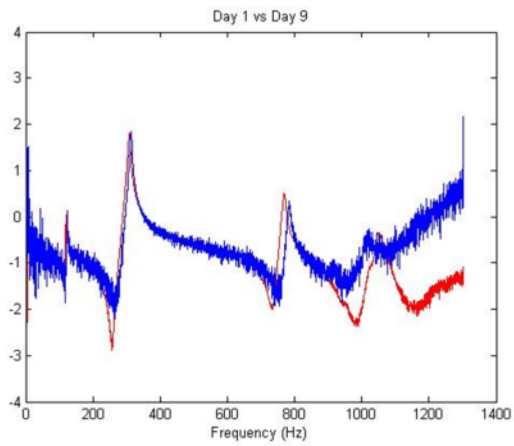

Figure 4.2 – FRF's from the 1st and 9th day

Although the poor quality of data from the first days, it can be seen that natural frequencies have changed. That change is even clearer in Table 4.1, where are the values for the three natural frequencies identified as well as the expected values which were obtained from the dynamic analysis on the frame without the steel bar, in software *GSA*. In Figure 4.3 are plotted all the obtained values. In Table 4.1 is also presented the percentage change compared to the first day, for each one of the three frequencies.

Table 4.1 – Natural Frequencies *vs* Time

Day	***1st N.F. (Hz)***	*Change (%)*	***2nd N.F. (Hz)***	*Change (%)*	***3rd N.F. (Hz)***	*Change (%)*	***GSA N.F. (Hz)***
1	123,02	0,00	313,44	0,00	783,92	0,00	1st – 129,4 2nd – 315,1 3rd – 786,4
2	123,02	0,00	313,76	0,10	785,19	0,16	
3	122,38	-0,52	312,49	-0,30	781,06	-0,36	
4	122,07	-0,78	311,22	-0,71	777,88	-0,77	
5	121,43	-1,29	310,90	-0,81	775,34	-1,09	
6	120,16	-2,33	308,35	-1,62	769,30	-1,87	
7	120,48	-2,07	308,99	-1,42	770,89	-1,66	
8	120,48	-2,07	309,31	-1,32	771,52	-1,58	
9	119,85	-2,58	308,67	-1,52	769,62	-1,82	

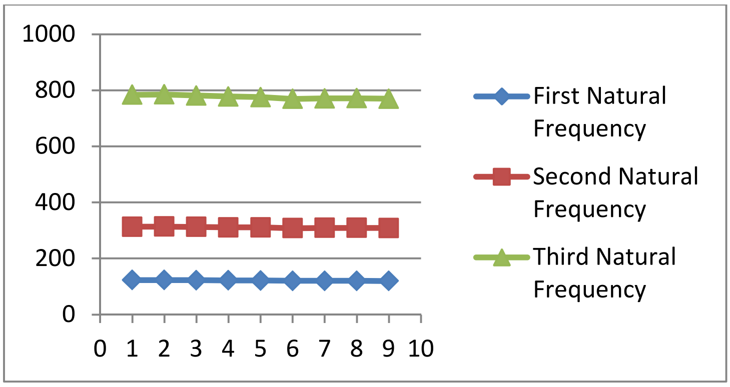

Figure 4.3 – Changes on Natural Frequencies due Time

The first inference to be taken from Table 4.1 is that the modeling in *GSA* was successful because the values obtained experimentally are almost identical to those obtained numerically.

Regarding changes to the natural frequencies of the frame, there was a decrease in all of them.

The 1st natural frequency verified the greatest decrease, totaling *2,58%* of the initial value, although this has remained constant during the first two days.

Except the 1st, 2nd and 3rd found an increase on the second day. Then, there is a nearly constant decrease in all of them until the 7th day, when there is an increase over two days, after back down.

Such changes are particularly evident in the following figures.

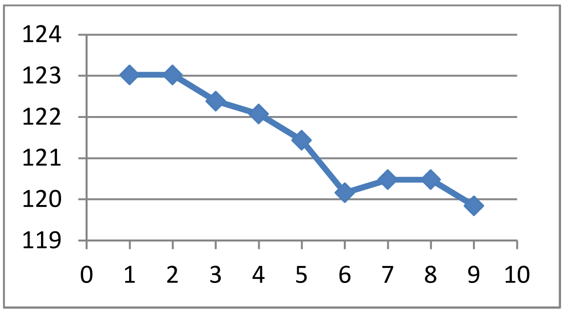

Figure 4.4 – 1st Natural Frequency Variation

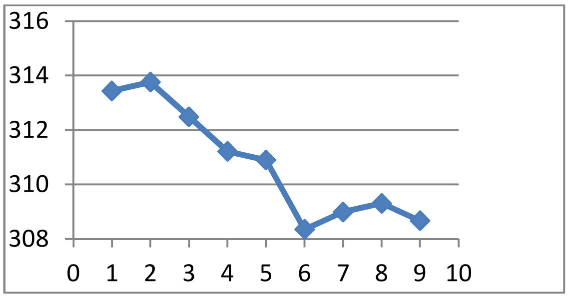

Figure 4.5 – 2nd Natural Frequency Variation

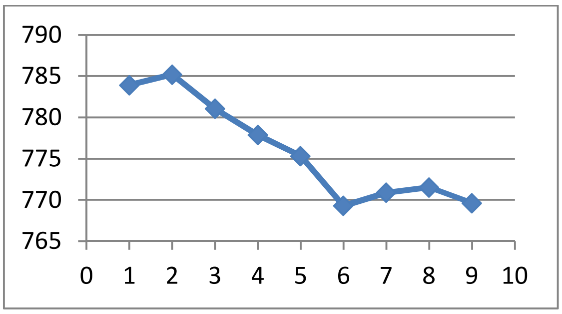

Figure 4.6 – 3rd Natural Frequency Variation

The frame was not deteriorated by the imposition of any static load during this test, this way such changes on this dynamic characteristic can be explained only by alteration in the mass of the structure. That could happen possibly by loss of water in the concrete, what could also change the stiffness of the system.

As noted above, changes in mass and stiffness of a system are directly related to alterations in its dynamic characteristics.

4.2. Frequency *vs* Load

Here it will be presented and analyzed the FRF’s obtained in dynamic tests, in each one of the frames, and for all load levels.

As already mentioned, after casting there were some deformations in frames due to the large amount of water in the concrete that later evaporated. These deformations were eventually different in each one of the frames, so is possible that they will also introduce different alterations in characteristics of each one of them.

As would be expected after the dynamic analysis carried out in the software *GSA*, two natural frequencies were identified in the studied sample rate. Please note that these are different from the natural frequencies presented in Section 4.1, since that, in these tests, it has been introduced the steel bar that is linked to the structure. This way it has obviously introduced changes to the natural frequencies of the structure.

In Figure 4.7 is shown a generic example of this structure FRF's. All others which have been collected in dynamic tests for the two frames in study are presented in *Appendix 6*.

After the observation of the FRF’s, the first question to put concerns with the fact that, although in the unloaded structure were only identified two natural frequencies, the application of static loaded introduced a third mode of vibration, as it can be seen in the Figure4.7. This new natural frequency seems to have derived from the 1st frequency, so that, henceforth, the three natural frequencies under study will be referred to as *1a*, *1b* and *2*.

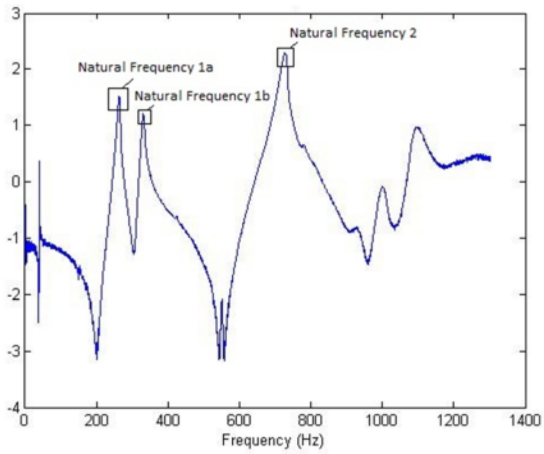

Figure 4.7 – Generic FRF of the Structure under Study

The three frequencies described above can be identified in all the FRF's in all the load levels, as can be seen in *Appendix 6*. However, while this happens, there were some changes in those graphics with the application of incremental static load and the consequent deterioration of the structure. The first and most important change refers to the variation of each natural frequency.

The second major change imposed by the load relates to the appearance of new peaks in the FRF's, which will also be analyzed. The study of this second phenomenon was carried out by a dynamic analysis in the direction perpendicular and by the visualization of some mode shapes considered relevant. Such can be seen later in sections 4.2.4 and 4.4.

The analysis of the variation of natural frequencies by increasing the static load will be done in the first place on each one of the frames, individually, and then it will be done a comparison between the two.

4.2.1. Frame 1

With the help of the FRF's presented in *Appendix 6*, it were measured the frequencies corresponding to each one of the peaks identified in those FRF's.

These values are presented below in Table 4.2.

Note that, for the load level of *1250 N*, values are not shown because it was found an error in data acquisition.

Table 4.2 – Natural Frequencies for Frame 1

Load (N)	***Natural Frequencies (Hz)***		
	1 a	***1 b***	***2***
0	-	270,84	746,41
125	261,62	304,86	725,11
250	263,85	330,93	728,29
375	263,21	340,46	728,93
500	236,85	356,04	732,74
625	263,21	359,22	733,69
750	249,23	336,65	693,64
875	252,72	350,32	706,99
1000	254,63	351,59	709,85
1125	258,45	360,81	719,07
1250	N/A	N/A	N/A
1375	260,67	367,16	734,97
1500	261,62	371,30	734,65
1625	260,99	375,43	737,19
1750	260,67	390,69	736,87
1875	259,08	393,55	735,60
2000	258,45	412,94	735,60
2125	257,49	418,35	735,92
2250	255,90	413,89	732,42
2375	254,95	415,17	731,79
2500	254,00	419,30	730,20
2625	253,36	418,98	728,93
2750	251,45	431,06	721,02
2875	250,50	420,89	725,75
3000	249,54	427,56	724,47
3125	249,54	431,70	732,52
3250	247,96	421,84	721,30
3375	247,00	422,48	719,71
3500	246,37	426,61	715,89
3625	246,68	423,43	716,53
3750	245,73	429,15	715,89
3875	244,78	425,66	717,48
4000	243,50	430,43	712,08

From this table can be seen, in the first place, an increase in both natural frequencies by the introduction of the steel bar to carry out these tests. Thus, comparing the values obtained for the load level where the frame was unloaded with the values shown in

Table 4.1, it turns out that both natural frequencies increased its value more than doubled. It should be noted that the third natural frequency from the Table 4.1 is now, with the introduction of the steel bar, out of the sample rate in study.

This proves the importance of the steel bar on stiffness of the structure.

Again taking into account the values of both natural frequencies for the load level where the frame is unloaded, and comparing these values with those obtained in dynamic analysis performed by the software *GSA*, which are presented in section 3.1.5., there is a large difference in values. Thus, contrary to what happened when the frame was modeled without the steel bar, this software was not fully effective in this case.

With the help of the Table 4.2 were made graphs of the variation of each one of the three natural frequencies identified with the static load applied. Figure 4.8 shows the natural frequency *1a*.

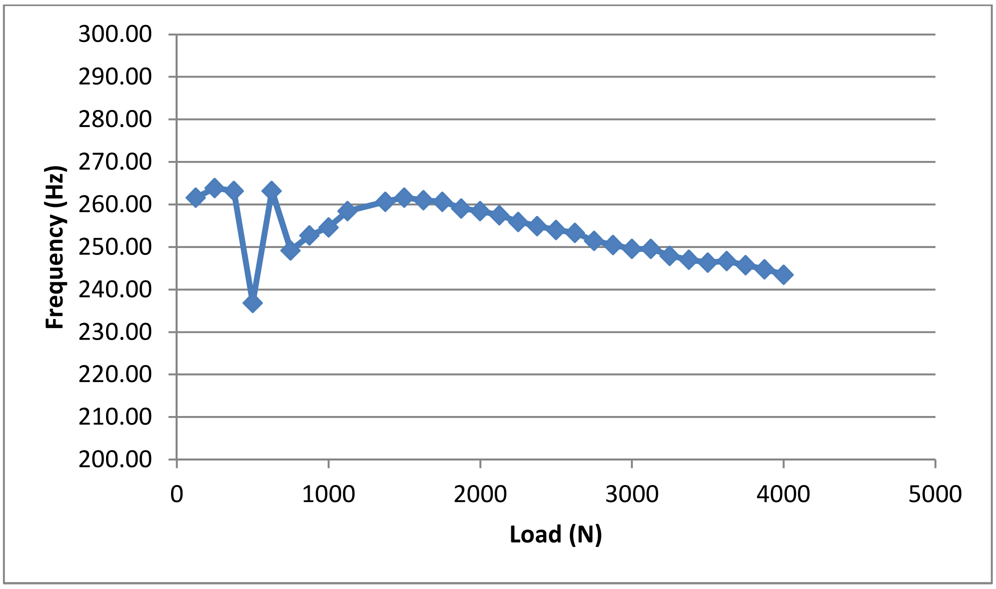

Figure 4.8 – Graph of Load against Natural Frequency 1a

The first approach to the graph shown above is that, after some gains and losses in the first load cycles, the first natural frequency tends to decrease in a nearly constant way as it approaches the load levels closer to failure.

For a better understanding, it is presented in Figure 4.9 a graph that represents the increase/decrease of the natural frequency *1a* in each load level.

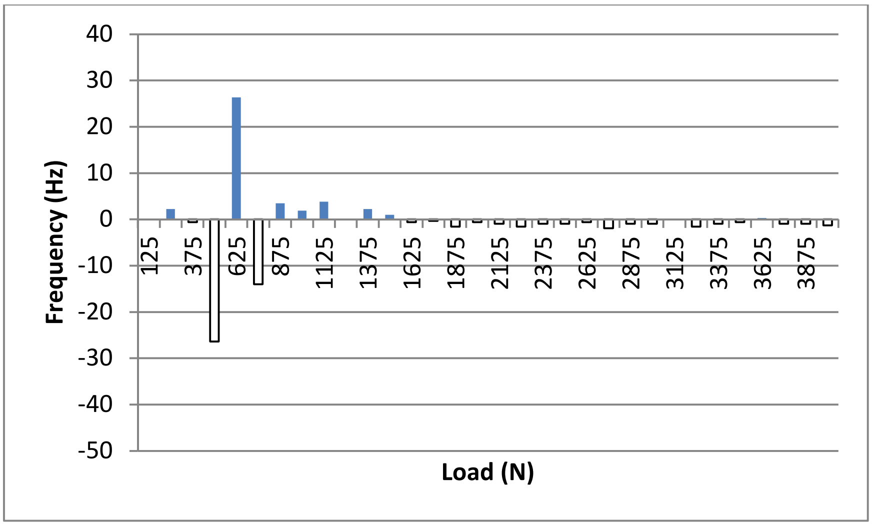

Figure 4.9 – Graph of Change of Natural Frequency 1a in each Load Level

It can be verified that, in general, there is a decrease of this natural frequency. In fact, there are very few load levels where its value decreases.

It is noteworthy that the greatest changes in its value happen for the initial load levels. It should be mentioned the load levels of *500 N, 625 N* and *750 N* are those where changes in this natural frequencies are higher. It is worth to remember that, in previous calculations, this is the loading level where the first crack on the structure occurs, although the large only have been observed for load levels closer to failure.

In Figure 4.10 is presented the graph of frequency against load referred to natural frequency *1b.*

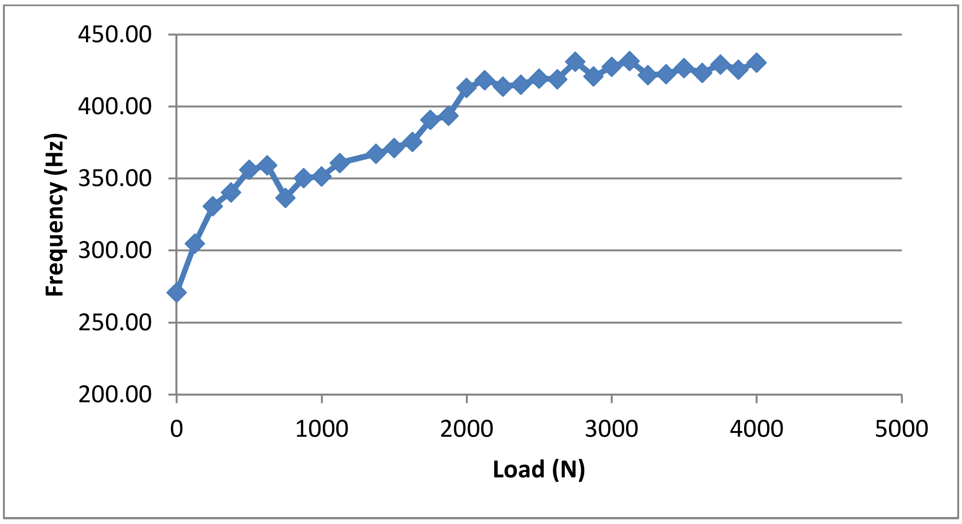

Figure 4.10 – Graph of Load against Natural Frequency 1b

Before the analysis of this graph, it should be remembered that this natural frequency is the one which derived from the first natural frequency, after the application of load in structure.

Thus, unlike the natural frequency *1a*, there is a general increase in almost load levels for this natural frequency.

Once again it is shown the graph of increase/decrease for each load cycle, regarding this natural frequency.

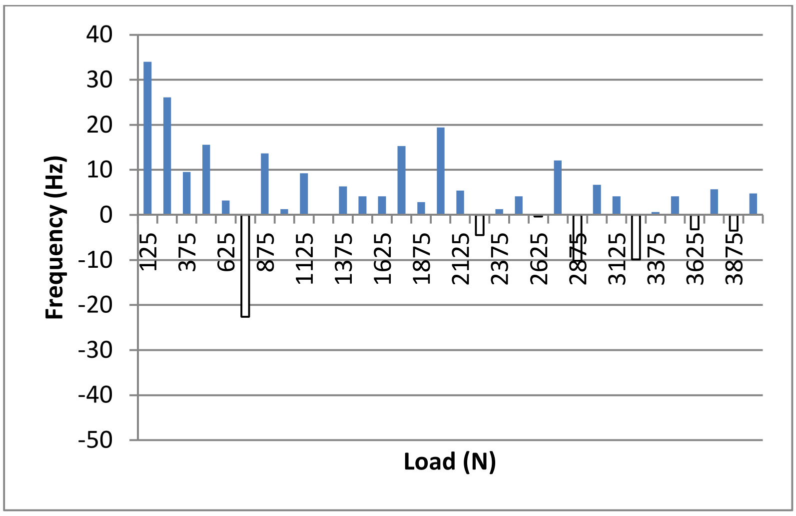

Figure 4.11 – Graph of Change of Natural Frequency 1b in each Load Level

This graph reinforces the idea of the increase of this natural frequency, with very few levels of load where it decreases.

Once again it appears the bigger changes occur for the initial load cycles.

For the natural frequency *2*, is presented below the graph frequency against load in Figure 4.12.

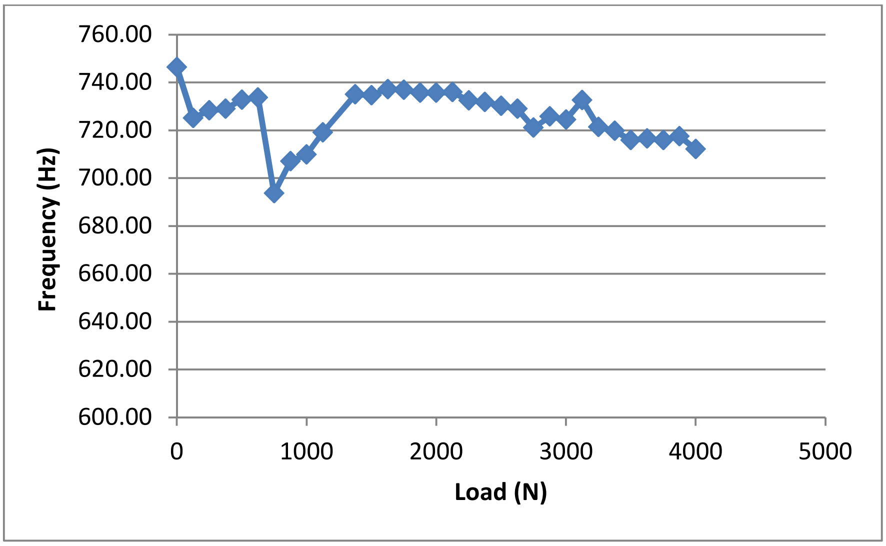

Figure 4.12 – Graph of Load against Natural Frequency 2

This frequency is from all three the one which shows the smoother variation, although it is notorious its decline as it approaches the failure of the frame.

Observing now the graph shown in Figure 3.13, there is the existence of various load levels that have not introduced major changes to its natural frequency.

Furthermore it is noted that the largest changes occur again for the lower load levels.

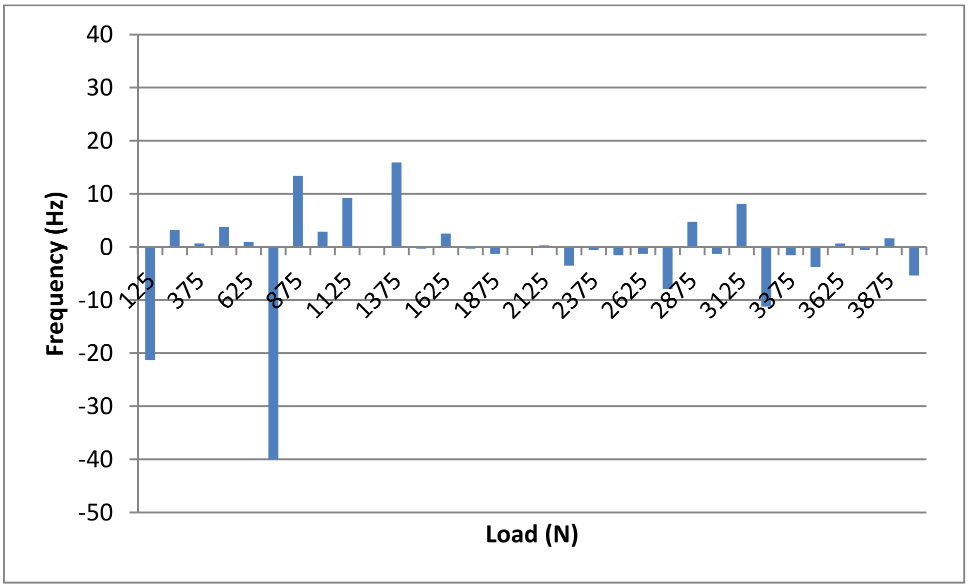

Figure 4.13 – Graph of Change of Natural Frequency 2 in each Load Level

As already mentioned the first and most important conclusion to withdraw from the FRF's of *Appendix 6* and from the table above relates to the emergence of a new mode shape with the application of the load.

This is even more evident in Figure 4.14, which shows overlaid FRF's, from load levels of *0 N* and *125 N*.

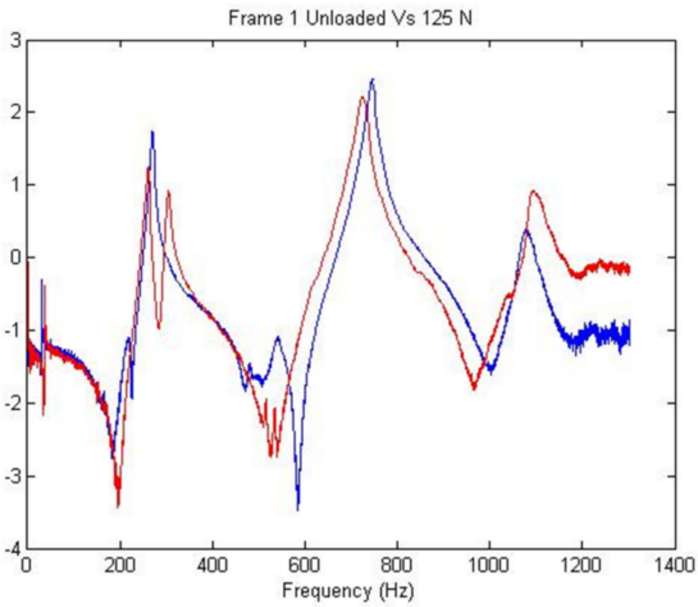

Figure 4.14 – FRF's from Load Levels of 0N (blue) and 125N (red)

This phenomenon will also be addressed during the analysis of mode shapes, however, is presented below the graph which reflects the difference between these two natural frequencies *1a* and *1b*, for each load level.

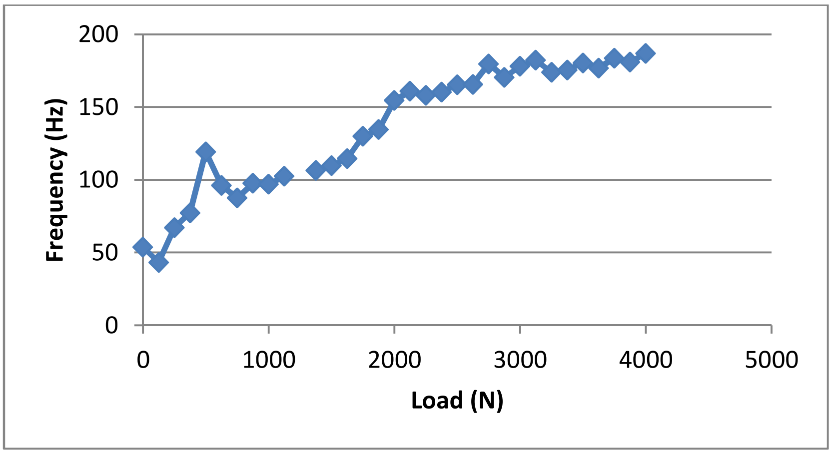

Figure 4.15 – Difference between Natural Frequencies 1b and 1a

It can be seen by observing the graph above that the bigger the applied static load on the frame is, the greater is the separation between the two natural frequencies which derived from the same.

There is clearly an increase almost constant of the difference between the frequencies.

Given the resistance features of the structure already known, namely the loads corresponding to the cracking and ultimate moment, there are presented in following figures overlaid FRF's for analyzing possible changes in modal characteristics in those load levels.

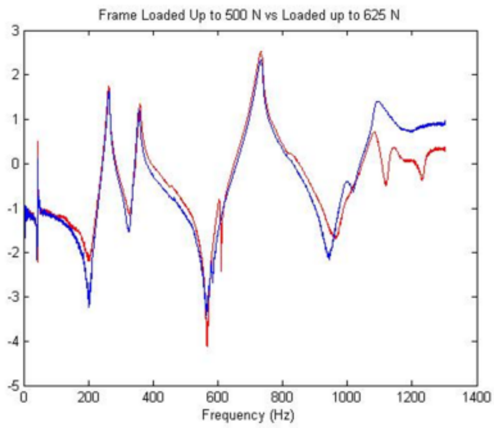

Figure 4.16 – FRF's from Load Levels of 500N (blue) and 625N (red)

The above figure represents the change that would be imposed by the load cycle where, theoretically, would appear the first crack. However, the change practically does not happen. Only for higher load levels were verified such cracks.

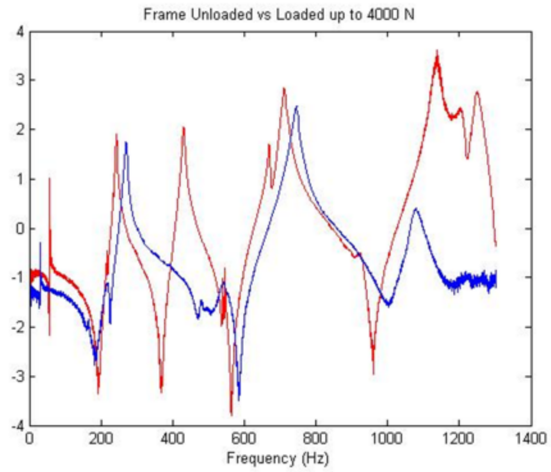

Figure 4.17 – FRF's from Load Levels of 0N (blue) and 4000N (red)

In Figure 4.16 is presented the change in the FRF of the structure, since the moment when it was unloaded until the maximum load that it has been subjected.

It is clearly evident the appearance of a second natural frequency from the first and that, in a load level near failure, the same seem that would happen with the natural frequency *2*.

4.2.2. Frame 3

As happened for the first frame, with the help of FRF's presented in *Appendix 6*, it were measured the frequencies corresponding to each one of the peaks identified in each of these FRF's. In Table 4.4 are presented the values collected for the frame 3.

It should be noted that, for load levels of *3500 N* and *4000 N* are not presented the values for the natural frequency *2*, because it were identified several peaks, not being possible the identification of such values. This is a theme that will be addressed when studying the mode shapes.

Table 4.3 – Natural Frequencies for Frame 3

Load (N)	***Natural Frequencies (Hz)***		
	1 a	***1 b***	***2***
0	257,17	276,25	747,26
125	274,02	431,06	751,18
250	273,70	347,14	751,18
375	272,11	364,94	751,18
500	269,88	365,09	748,53
625	269,89	364,94	747,68
750	270,53	380,20	750,96
875	269,89	384,65	751,18
1000	268,62	384,33	749,27
1125	274,02	390,37	745,45
1250	268,30	396,41	745,45
1375	262,26	402,13	745,45
1500	267,03	395,46	746,73
1625	262,58	404,68	738,46
1750	262,26	404,99	738,48
1875	261,62	411,03	735,96
2000	259,26	408,31	734,58
2125	259,40	409,13	732,10
2250	258,45	412,62	730,83
2375	257,81	407,85	729,56
2500	256,08	434,91	727,72
2625	256,54	409,44	728,92
2750	250,82	417,07	718,75
2875	249,86	415,80	718,12
3000	249,86	420,89	719,07
3125	249,54	417,07	717,16
3250	248,59	417,39	714,30
3375	246,68	419,93	709,21
3500	246,64	421,57	-
3625	246,37	422,16	699,36
3750	246,68	419,93	708,58
3875	240,01	417,07	686,64
4000	230,26	427,70	-

Regarding the influence of the introduction of the steel bar, as happened for the frame 1, it was found an increase for more than the double of each one of the natural frequencies. This can be detected by comparing the values of the first row with those presented in Table 4.1.

Now comparing the values obtained in dynamic analysis carried out in *GSA*, which are presented in section 3.1.5., with those presented in the first row of the Table 4.3, here too there is a big difference on the natural frequencies.

From this table it can also be concluded that, contrary to what was seen in the frame 1, when the structure was unloaded, there were already distinguished the natural frequencies *1a* and *1b*. This only happened in the first frame after the start of the application of load and it may be explained, for this frame, by the fact that the steel bar was probably doing some strength against the side beams.

This is highlighted in Figure 4.18, where it is shown the FRF of the structure unloaded.

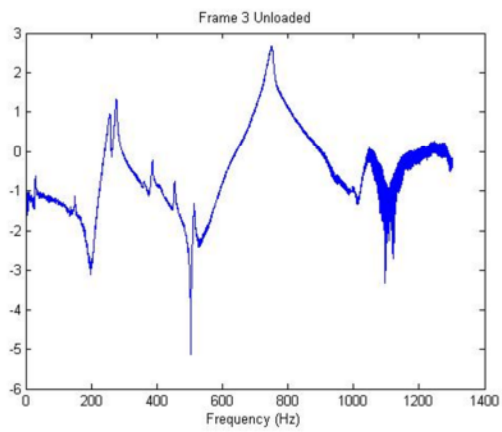

Figure 4.18 – FRF from Frame 3 Unloaded

In Figure 4.19 it is presented the graph of the variation of the natural frequency *1a* with the static load applied.

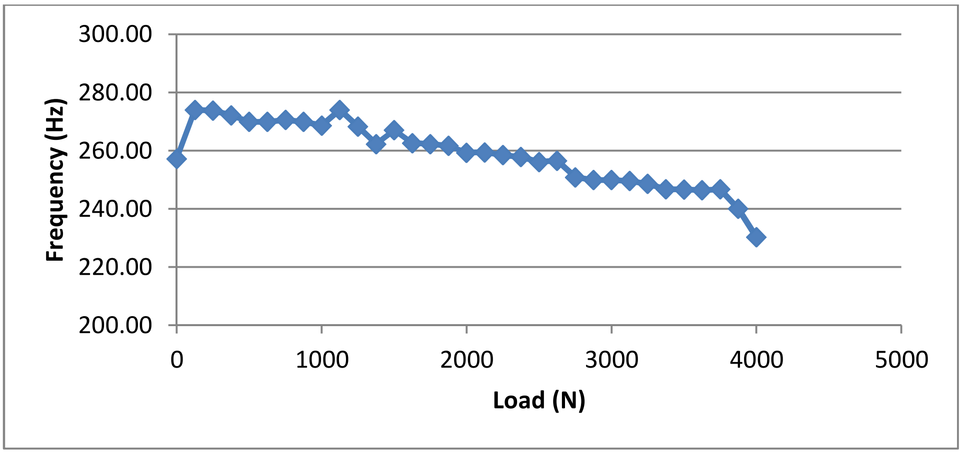

Figure 4.19 – Graph of Load against Natural Frequency 1a

As noted in the previous frame, here too is an almost constant decrease of this frequency with the increase of the static load.

In Figure 4.20 is shown the increase/decrease of this natural frequency for each load cycle.

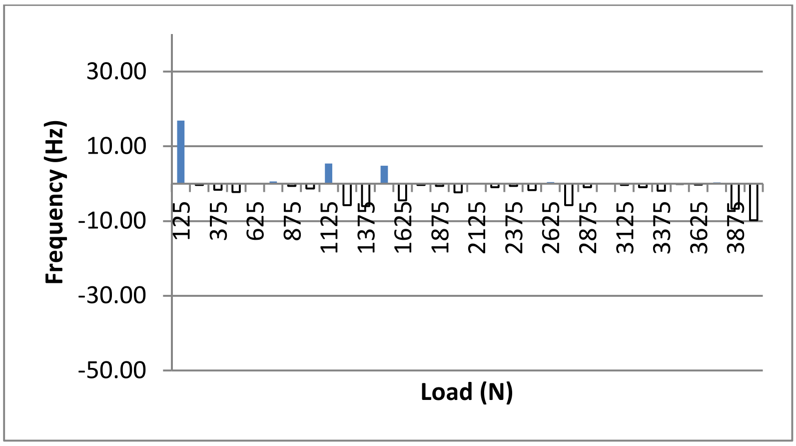

Figure 4.20 – Graph of Change of Natural Frequency 1a in each Load Level

There is a decrease in almost load levels. However, the biggest change is the increase of the frequency when the static load was applied for the first time.

It should be also noted the great decrease found in the levels near failure.

For the natural frequency *1b*, is presented in Figures 3.21 and 3.22 the study of the variation of the same with the static load applied.

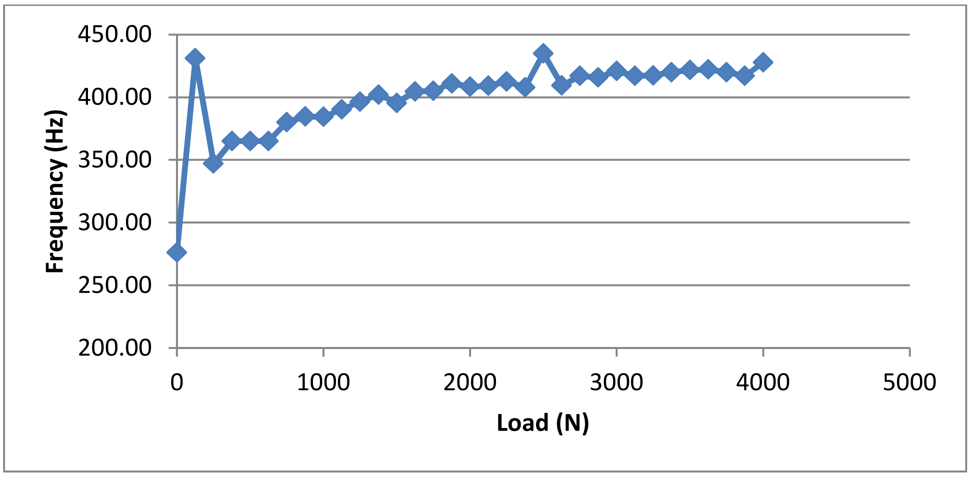

Figure 4.21 – Graph of Load against Natural Frequency 1b

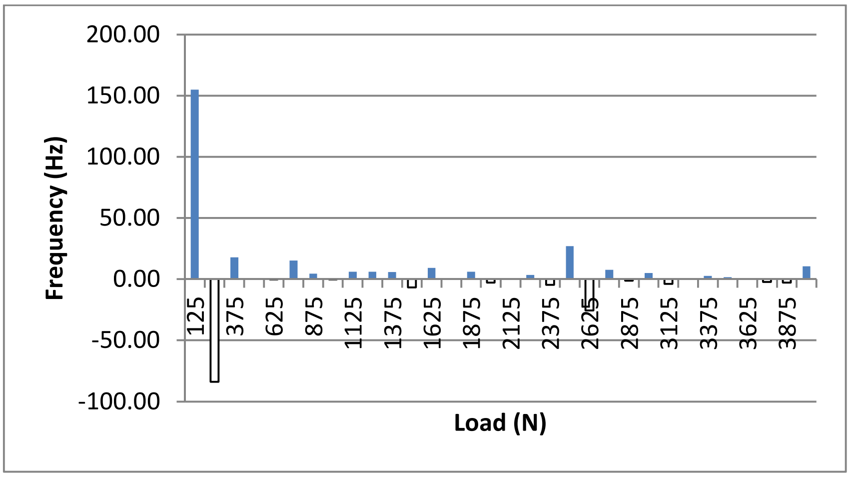

Figure 4.22 – Graph of Change of Natural Frequency 1b in each Load Level

From the analysis of both graphs presented in two figures above, it can be found the increase of this natural frequency in an almost constant way until the levels of load near failure.

The main changes occur in the first two levels of loading and it should be mentioned that, as it already happened in the natural frequency *1a*, the initial application of the static load imposed the greater increase in this frequency.

The graphs in Figures 4.23 and 4.24 are referred to the natural frequency *2* and to its change due to the increase of the static load applied on the structure.

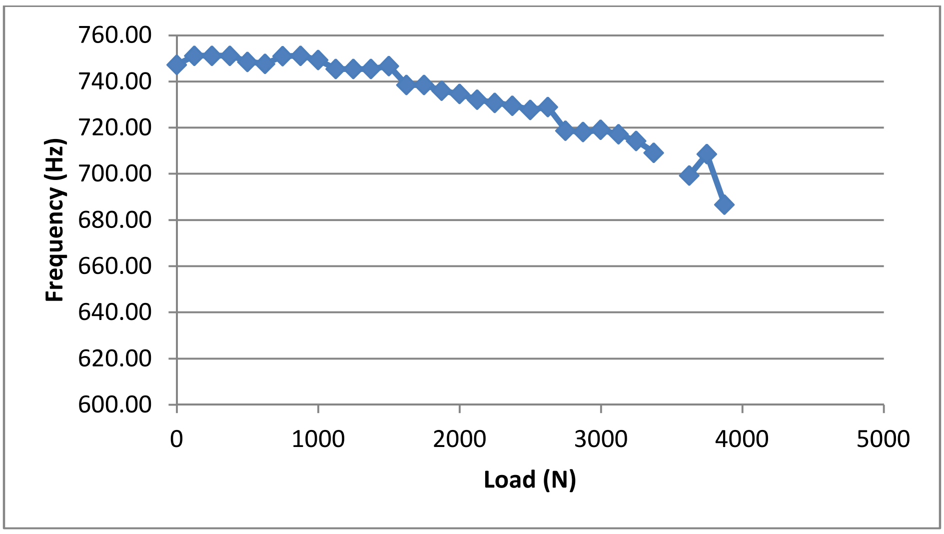

Figure 4.23 – Graph of Load against Natural Frequency 2

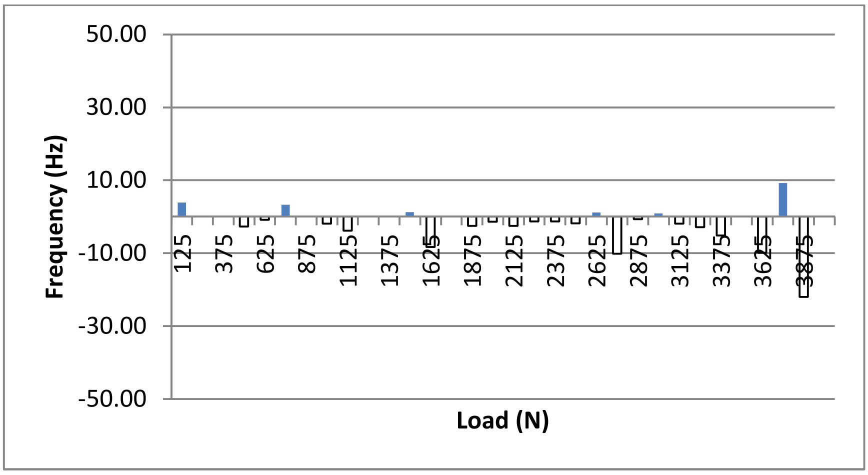

Figure 4.24 – Graph of Change of Natural Frequency 2 in each Load Level

It can be seen an almost constant decrease in this frequency, and this decrease occurs in practically all load levels.

As it happened in the frame 1, this was the natural frequency where the changes imposed by the static load were lower. This way, it can be seen a much smoother decrease of this natural frequency, when compared to the decrease of the natural frequency *1a* and the increase of the natural frequency *1b*.

Regarding the natural frequencies *1a* and *1b*, here too there is an increase in its difference with the increase of the load. This is shown by the graph presented in Figure 3.25.

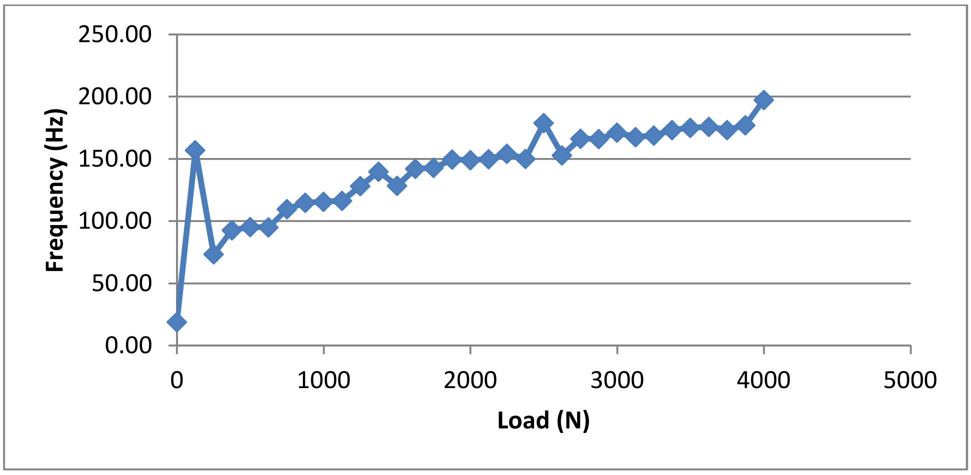

4.25 – Difference between Natural Frequencies 1a and 1b

It should be noted that, for this frame, the first load level was much more important. It can be seen a large separation between the two natural frequencies after this load cycle.

After that there is a big decrease on the second load level, before the difference increases again until load levels near failure.

The importance of the fist load level, when the static load was introduced to the structure, is visible in the following figure, which shows overlaid FRF's corresponding to the unloaded structure and to a load level of *125 N.*

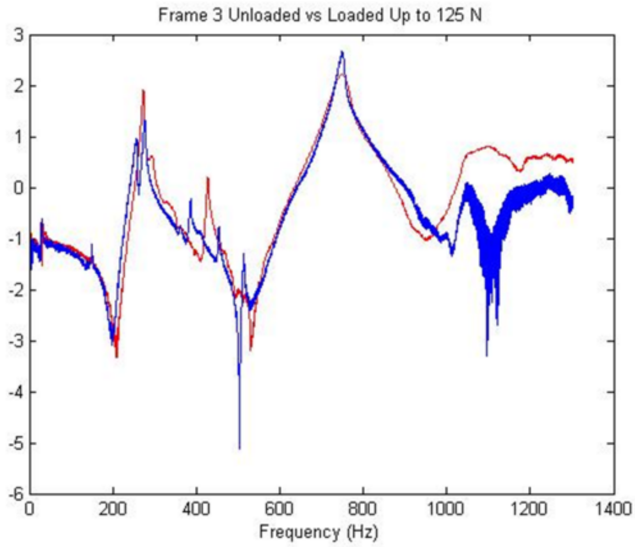

Figure 4.26 – FRF' from the Unloaded Frame and Loaded Up to 125 N

It is proved with this figure the huge difference that the initial application of the load introduces on the first two natural frequencies.

As it was verified on the first frame, the load cycle where, theoretically, would begin the cracking of this structure, has not introduce almost any difference in FRF of the structure. It can be seen in *Appendix 6* by observing the FRF's of the load levels of *500 N* and *600 N.*

In Figure 3.27 can be verified the total change imposed by the maximum load applied. There are represented the overlaid FRF's corresponding to the structure unloaded and to the load level of *4000 N.*

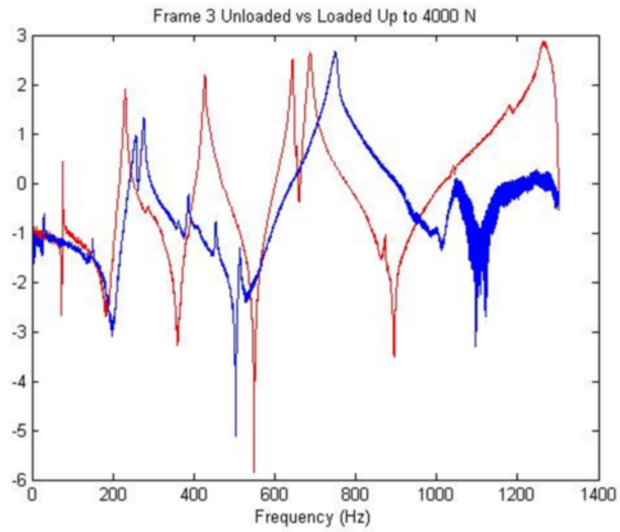

Figure 4.27 – FRF'S from the Unloaded Frame (Blue) and from the Load Level of 4000 N

It should be noted from the load level near failure the total separation of the first natural frequencies in both *1a* and *1b*, as well as the the second, which will be discussed later, at the analysis of mode shapes.

4.2.3. Frame 1 vs Frame 3

Here it will be addressed the consistency of the data obtained. To this end, it are presented in the following figures the overlaid graphs of each one of the natural frequencies, for both frames. These frequencies were already analyzed previously, although individually.

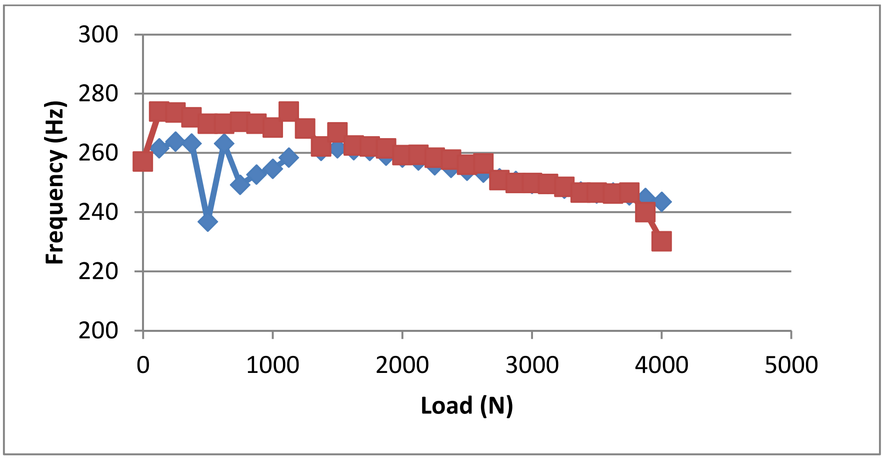

Figure 4.28 – Graph of Load against Frequency 1a for both Frames

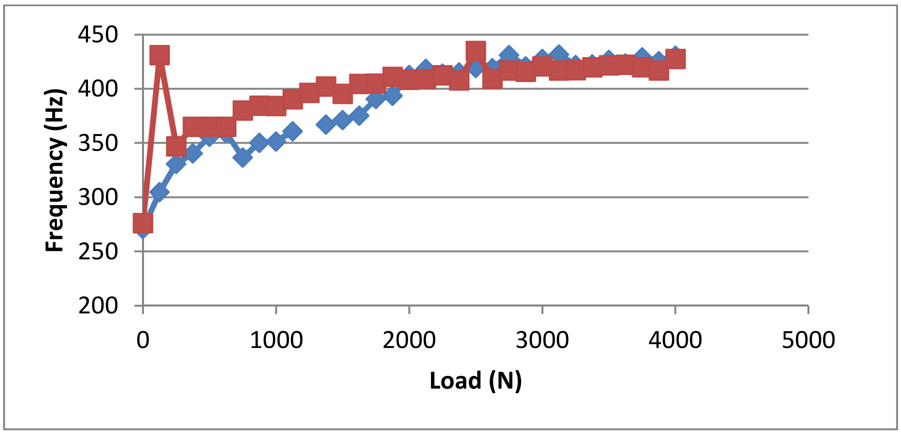

Figure 4.29 – Graph of Load against Frequency 1b for both Frames

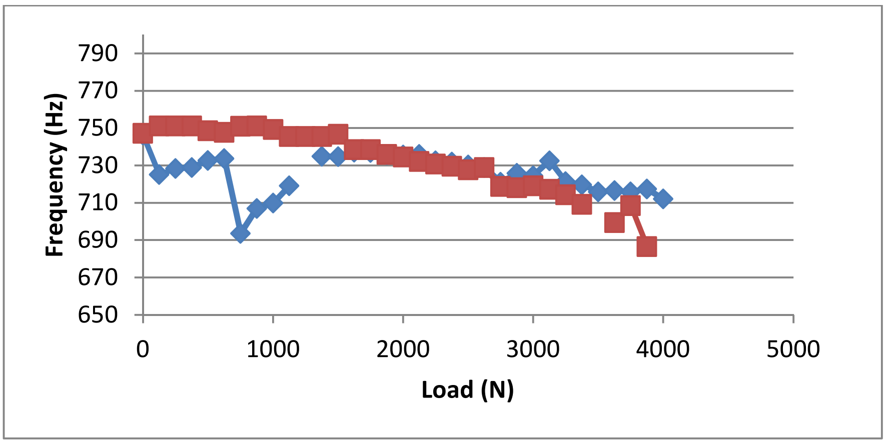

Figure 4.30 – Graph of Load against Frequency 2 for both Frames

By observing the graphs above but also Tables 4.2 and 4.3 it can be stated that the natural frequency *1a* has decreased more than 10% in both frames, more specifically 10,1% in frame 1 and 10,5% in frame 3.

The natural frequency *1b* has increased almost 59% in frame 1 and more than 35% in frame 3.

The natural frequency *2* has decreased almost 5% in frame 1 and more than 8% in frame 3.

Besides that, it should be noted that all graphs present the same trend for both frames, which confirms even more the consistency of data.

However, the initial load levels have introduced major changes in frame 1, mainly for what is observed in graphs of natural frequencies *1a* and *2.* In addition, the introduction of the static load seemed to have a greater influence in frame 3. That can be observed in the first two graphs, where is verified a large increase in natural frequencies *1a* and *1b.*

It can be seen that the frame 1 presents lower values in all three natural frequencies on the first load levels.

Finally, it is noted that the first two natural frequencies show very similar values for both frames in loading levels near failure.

4.2.4. Analysis in Direction Perpendicular

As is shown in graphs presented in *Appendix 6,* there are some peaks in the FRF's that do not match to any natural frequencies already identified.

For a better understanding of the phenomenon, another dynamic analysis was carried out, this time in the direction perpendicular to the one that was being tested. Other measurements were made, with the excitation taking place at the same point – *point 5* – as well as the position of the accelerometer. However the analysis was carried out in the *plane xz* in order to verify the possibility of mode shapes in that plane whose natural frequencies could explain some of the peaks seen on the FRF's obtained.

These tests were made only for a few load levels and the results are summarized in Table 4.4.

Table 4.4 – Analysis in Direction Perpendicular

Load (N)	Natural Frequencies (Hz)		
	1 a	1 b	2
0	133,20	300,73	715,89
500	116,35	278,47	634,51
1000	114,12	291,51	664,39
1500	122,07	308,04	690,78
2000	123,02	315,67	705,40
3750	130,02	331,88	733,69

With the help of the Table 4.4 it will be tried an explanation for some of the peaks verified in some load levels in both frames.

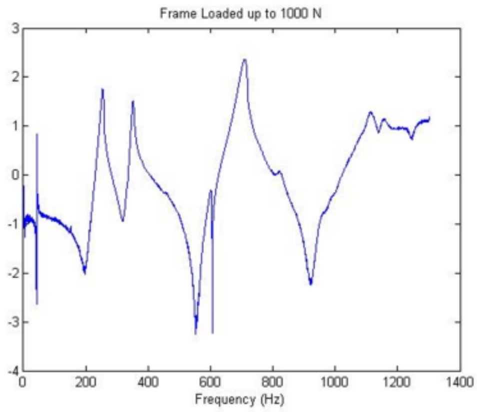

Figure 4.31 – FRF for Frame 1 Loaded Up to 1000 N

The FRF for the load level of *1000 N*, on frame 1 has a small peak after *600 Hz*, which may correspond to natural frequency of the third mode shape in direction perpendicular to the one in study.

This also may be important on the observation of the FRF of the load level of *3750 N*, on frame 1, where it can be seen a peak near the natural frequency *2*.

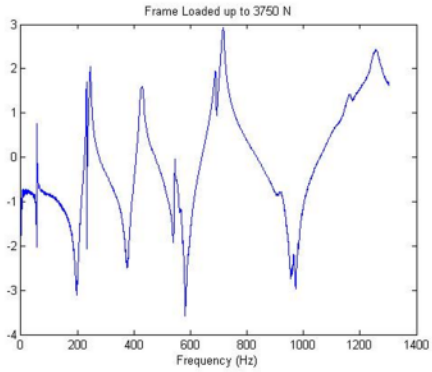

Figure 4.32 – FRF for Frame 1 Loaded Up to 3750 N

For the frame 3, there is also a peak near *600 Hz*, in the FRF of the load level of *1500 N*.

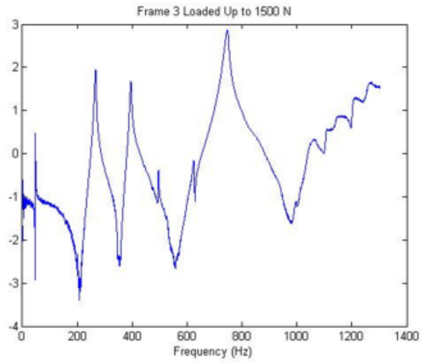

Figure 4.33 – FRF for Frame 3 Loaded Up to 1500 N

4.3. Damping *vs* Load

In *Appendix 7* are presented the damping values collected for each natural frequency in study and for all load cycles, in each one of the frames. Note that for the frame 3 there are not presented these values for the load levels of *3500 N* and *4000 N* because there were identified other peaks on corresponding FRF's, so that may correspond to other mode shapes. These cases will be discussed in section 4.4.

Values presented in *Appendix 7* allowed the construction of the graphs below, for each frame.

4.3.1. Frame 1

In following figures are presented the graphs of damping against load, of the three mode shapes identified and whose natural frequencies – *1a*, *1b* and *2* – have been already addressed in the previous section.

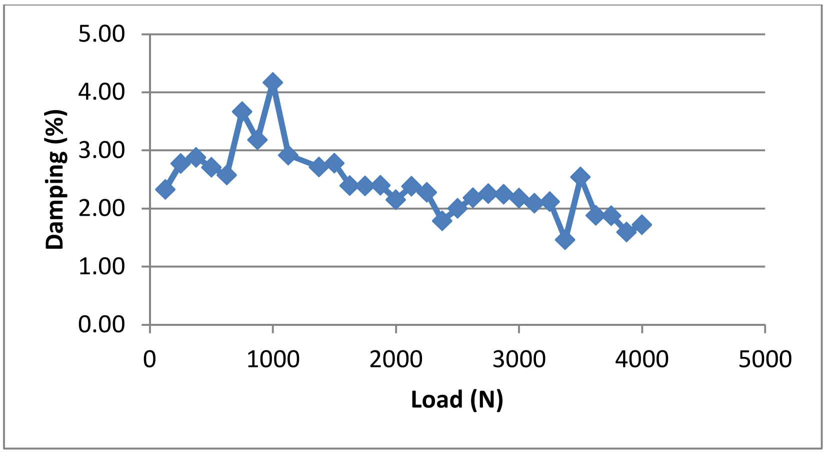

Figure 3.34 – Damping against Load for Natural Frequency *1a*

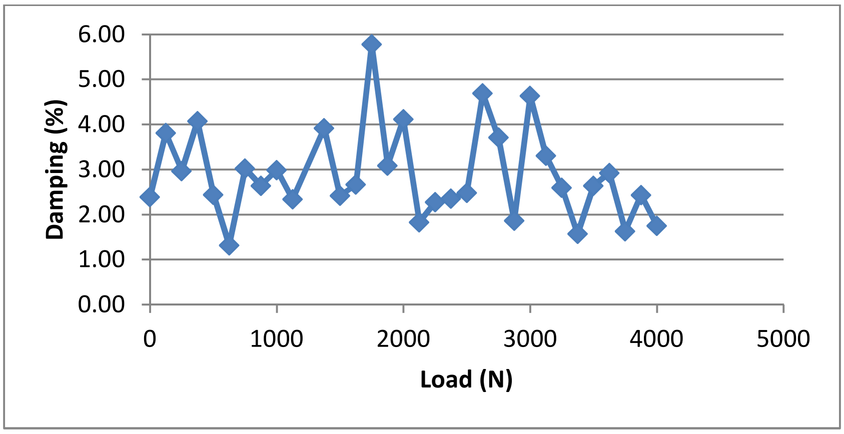

Figure 3.35 – Damping against Load for Natural Frequency *1b*

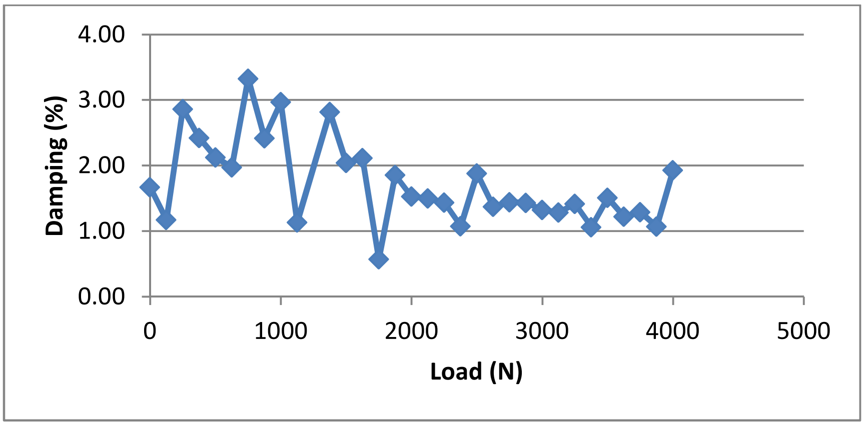

Figure 3.36 – Damping against Load for Natural Frequency *2*

Regarding the variation of damping with the increasing static load, it seems that there is no correlation between them. This happens for the three natural frequencies. However it is particularly notorious for natural frequency *1b.*

On the natural frequency *1a*, although changes are not constant with the increasing load, it seems to be the least affected in terms of damping.

Both natural frequencies *1a* and *2* show major variations in the first load levels and for load cycles near failure that change is not as expressive.

It may be also stated that this is a structure considerably damped, as it almost always has values near 1,5% of damping for the natural frequency *1a*, 3% for natural frequency *1b* and 1,5% for natural frequency *2.*

4.3.2. Frame 3

In Figures 4.37, 4.38 and 4.39 are presented the graphs of damping against load of each one of the three mode shapes identified.

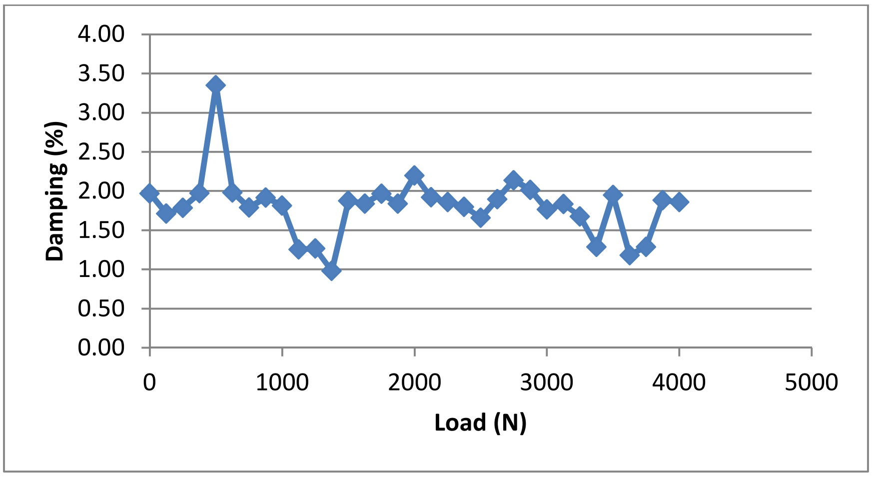

Figure 4.37 – Load against Damping for Natural Frequency *1a*

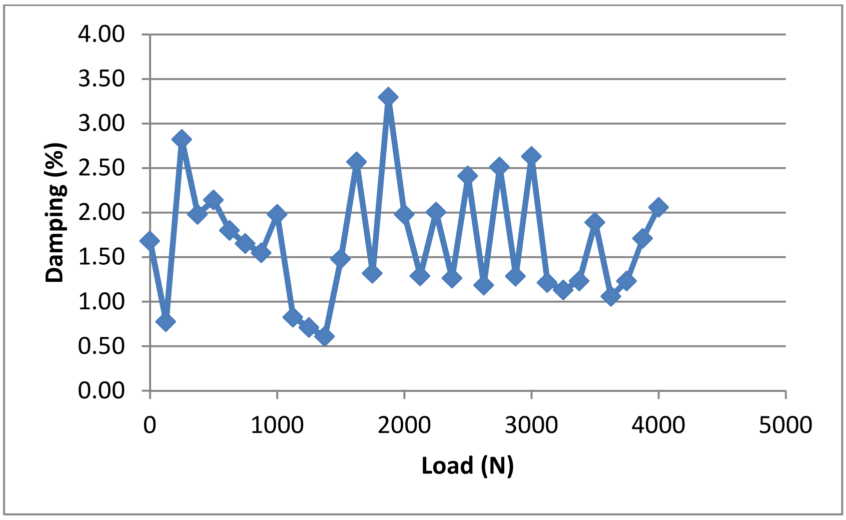

Figure 4.38 – Load against Damping for Natural Frequency *1b*

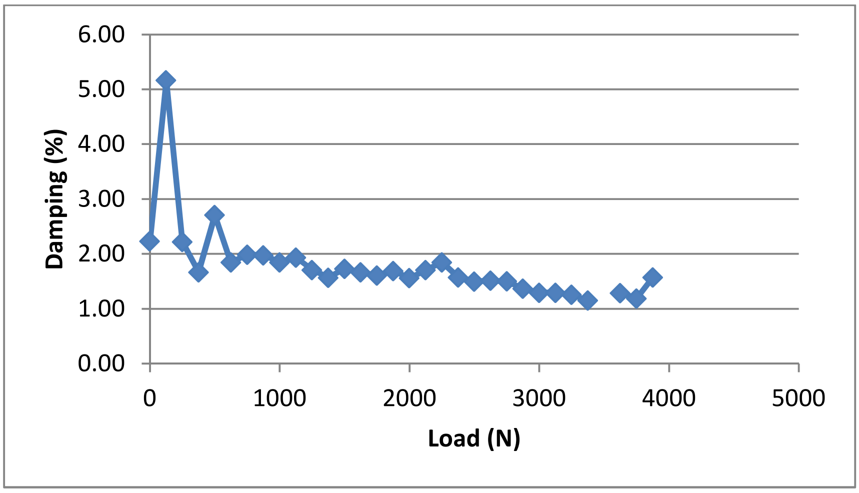

Figure 4.39 – Load against Damping for Natural Frequency *2*

Once again it is difficult to find a correlation between the load cycles and the values of damping obtained.

Again the natural frequency *1b* displays a constant alternation between growth and decline in the value of damping. Also, the natural frequency increases and decreases several times with the static load.

The natural frequency *2* presents a large increase on damping by the introduction of the static load, but after that its changes on damping are much smaller, keeping always between 1 and 2%.

4.3.3. Frame 1 vs Frame 3

After analyzing the damping data from each one of the frames individually, it will be done a comparison between them, trying to find some consistency on data.

Figures 4.40, 4.41 and 4.42 present overlaid graphs of damping against load for both frames, each one of those graphs for one of the three mode shapes.

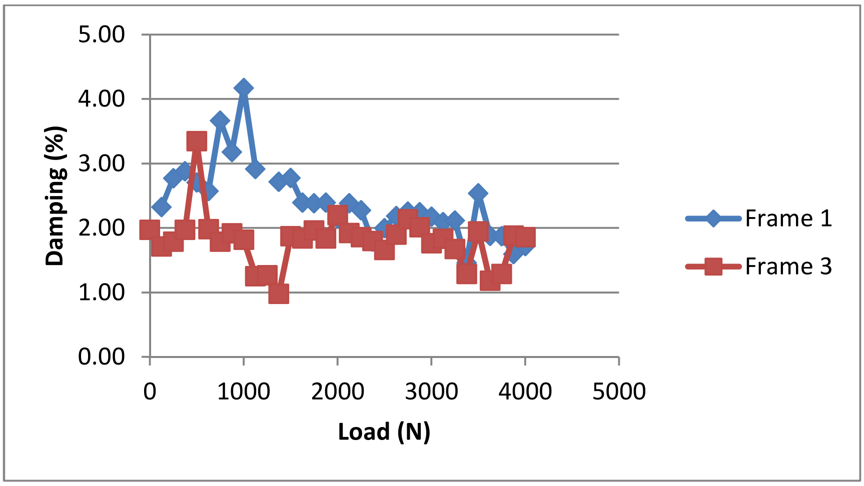

Figure 4.40 – Graph of Load against Damping for Natural Frequency 1a for both Frames

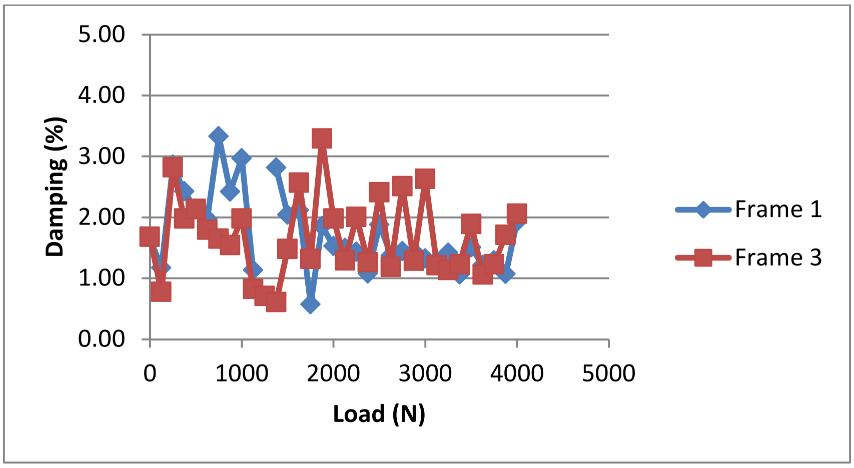

Figure 4.41 – Graph of Load against Damping for Natural Frequency 1b for both Frames

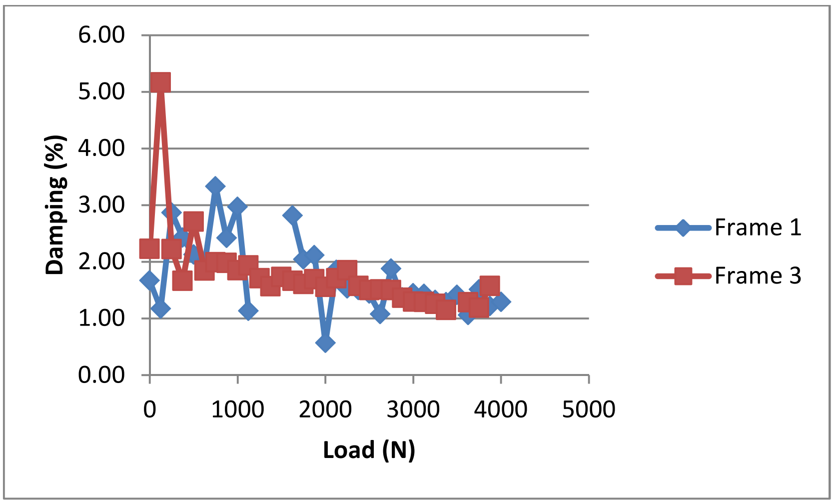

Figure 4.42 – Graph of Load against Damping for Natural Frequency 2 for both Frames

After there was not found a correlation between the loading and damping for each one of the two frames, the comparison between the two frames show that it does not seem to be a good match between them. This may reveal that the method of determining this modal characteristic may not be the best.

Even so, there seems to be an approach between the values of the natural frequencies *1a* and *2*, for load levels near failure. However, values of damping for the natural frequency *1a* are always higher in frame 1.

The damping of the natural frequency *2* seems to have been more influenced by the application of the static load on frame 3 than on frame 1, where it is verified a greater variation for the rest of the load levels.

Regarding the natural frequency *1b*, this varies constantly between increase and decrease of the damping values on both frames. However, such variation does not occur in the same way.

One thing that can be concluded by observing these three graphs is that damping changes in a different way for each one of the natural frequencies.

Once again it should be mentioned that this is a structure with a considerable damping.

4.4. Mode Shapes *vs* Load

As already mentioned, for some load levels, there are some peaks in the FRF's without explanation. In an attempt to a better understanding of that phenomenon, in addition to the dynamic analysis in direction perpendicular to the one which is in study which was already presented, there were reproduced mode shapes of some load levels which seemed to be relevant. This was made in order to try to identify new mode shapes that could appear with the increase of the static load.

In addition, it were studied some possible changes to the form of mode shapes.

To this end, it was used the software *Icats* and also the FRF's collected at different points of the frame, for the same load level.

By observing the FRF's of each frame, it can be already stated that the results obtained for both of them present some differences. Thus, since the mode shapes that should be addressed are different between the two frames, it will be study each structure individually.

4.4.1. Frame 1

In this section it will be analyzed mode shapes of frame 1 for load levels that seemed relevant, by observing its FRF's.

It were first analyzed mode shapes of the frame when was unloaded, so that they could be compared to those obtained from *GSA.*

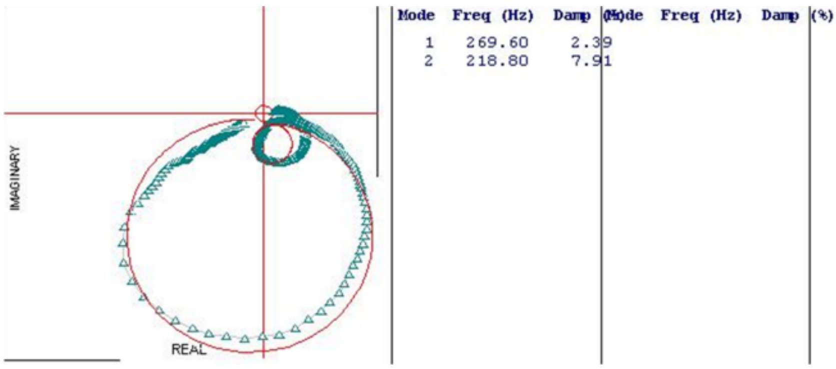

Figure 4.43 – Natural frequencies 1 a and 1 b identified on Icats

Note that the software *Icats* identified for this frame both mode shapes corresponding to natural frequencies *1a* and *1b,* although these have not been identified by observing the FRF's. However, that could happen due to the fact that the steel bar was already in the frame, applying load, even if it was minimal. So the first of these may not correspond to a mode shape, for this level of load.

In the following figure are represented those two mode shapes, and another one corresponding to the natural frequency *2.*

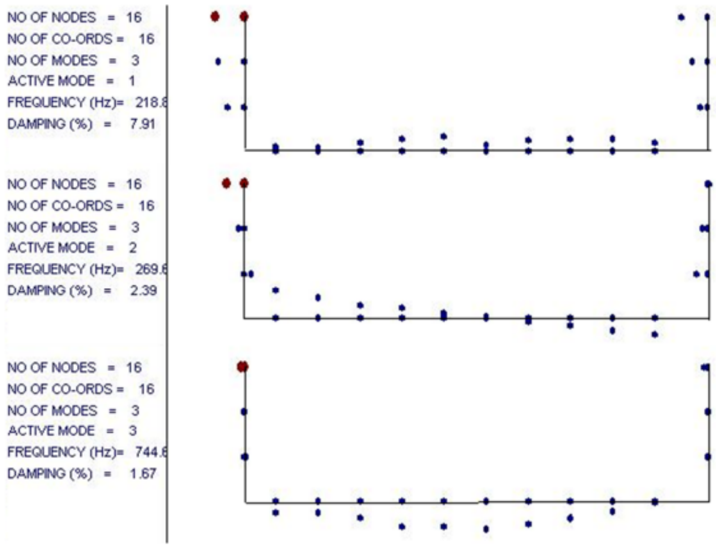

Figure 4.44 – Mode Shapes of the Unloaded Frame 1

It should be noted that the mode shape number 2 is in many ways similar to that obtained by *GSA* that is presented in Figure 3.30, while the third corresponds to that shown in Figure 3.31.

Then it were also analyzed mode shapes for the load level of *2500 N*, because it was observed the appearance of small peaks between frequencies *1b* and *2*, possibly due to the damage created by the higher load applied.

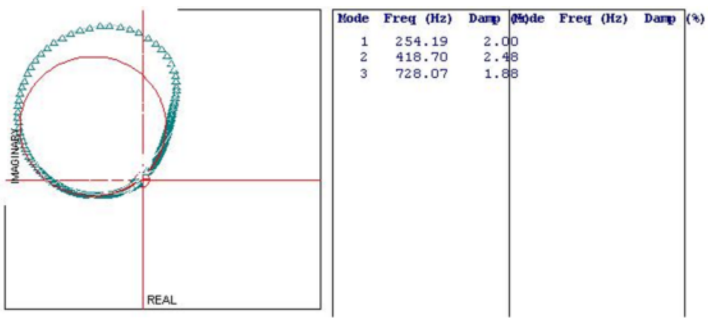

Figure 4.45 – Mode Shaped Identified by Icats for Load Level of 2500 N

As it can be seen, were not identified new mode shapes besides the three already known, so that the peaks shown in the FRF corresponding to this level are not referred to new mode shapes.

This was also made for load levels of *3500 N* and *4000 N*, not being identified new mode shapes for none of them.

It should be mentioned that in general, FRF's from this frame had shown some quality, so there was no need to study other load levels.

Regarding the change of mode shapes already identified, Figures 4.46 and 4.47 show reproductions of each one of the three mode shapes of the first frame, on the load levels of *1000 N* and *4000 N*.

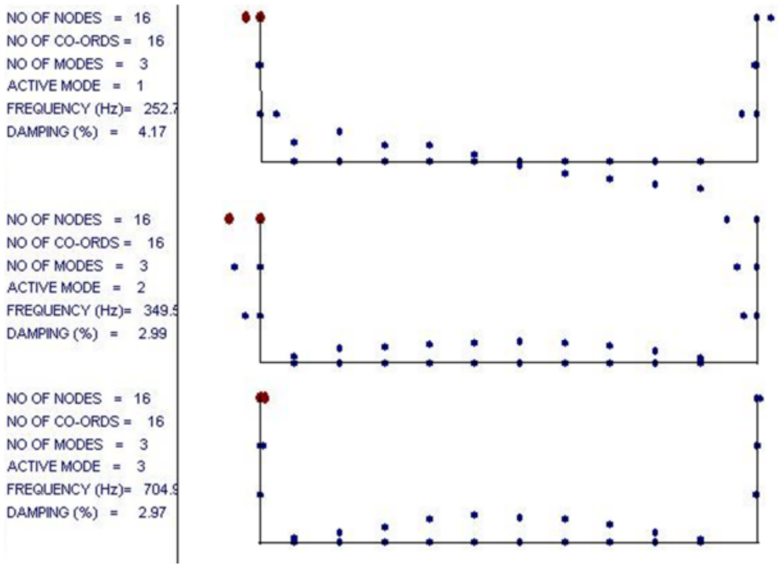

Figure 4.46 – Mode Shapes of Frame 1 after Loaded Up to 1000 N

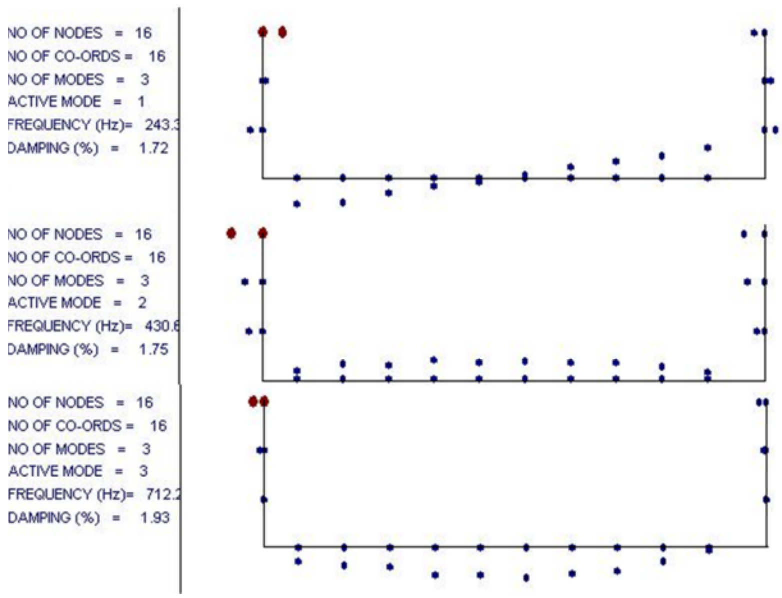

Figure 4.47 – Mode Shapes of Frame 1 after Loaded Up to 1000 N

Comparing each one of the modes for both load levels, there does not seem to be any change between them.

It is also worth noting that, although the second mode has appeared after loading the structure, deriving from the first, it has a much more similar shape to the third.

It can also be verified that the first mode shape from the Figure 4.44 – unloaded frame – should not in fact correspond to a mode shape, as suspected.

4.4.2. Frame 3

Although it has been proven consistent results between the two frames in what concerns to changes on natural frequencies, this structure has presented FRF's that raised more questions. This happened because, as it can be seen in *Appendix 6*, its FRF's show several peaks in many load levels.

In this section it will be find an explanation for this, trying to match some of those peaks to new mode shapes, as it was already tried in frame 1.

The first FRF to be analyzed is the one corresponding to the unloaded structure, which presents several peaks which do not match to any of the already identified natural frequencies.

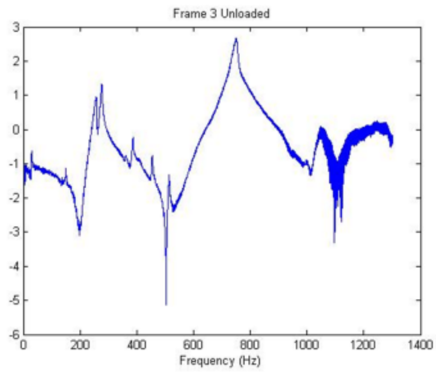

Figure 4.48 – FRF from Frame 3 Unloaded

The software *Icats* has identified five mode shapes, corresponding to the peaks shown in the FRF from Figure 4.48. These mode shapes are presented then.

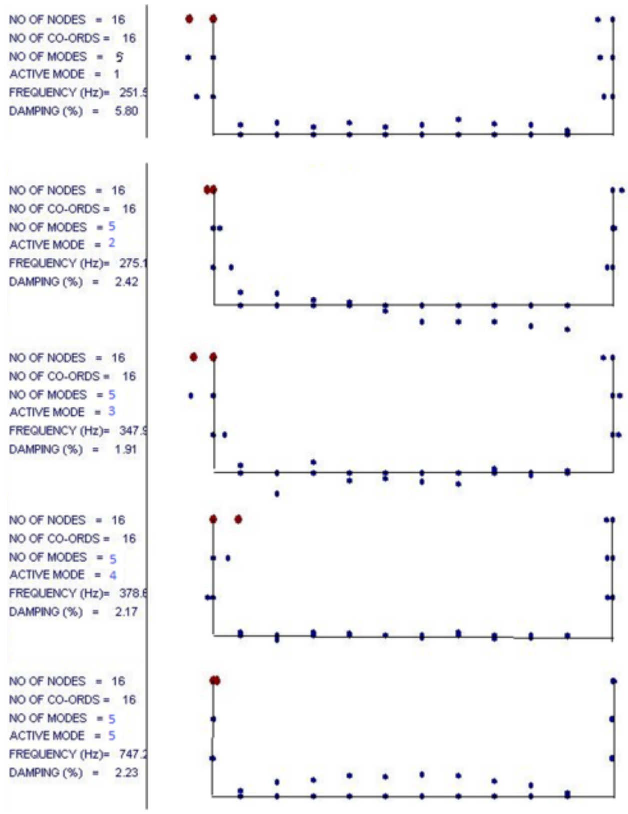

Figure 4.49 – Mode Shapes Identified on Icats for Frame 3 Unloaded

It should be noted that, from the five identified mode shapes, only the second and the fifth were identified in both *GSA* and frame 1, when the structure was unloaded. In addition, for the next load level – *125 N* – only the already known three mode shapes were identified, so this case may have happen due to a possible error during the measurements.

Then it was proceeded to the analysis of the mode shapes for the load level of *500N*, whose FRF is shown in Figure 4.50.

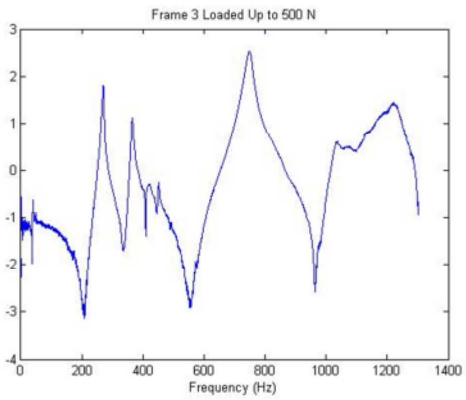

Figure 4.50 – FRF from Frame 3 Loaded Up to 500 N

For this FRF it has not been identified a new mode shape and, therefore, any explanation for the peak in the area after *400 Hz*, as can be seen in the following figure.

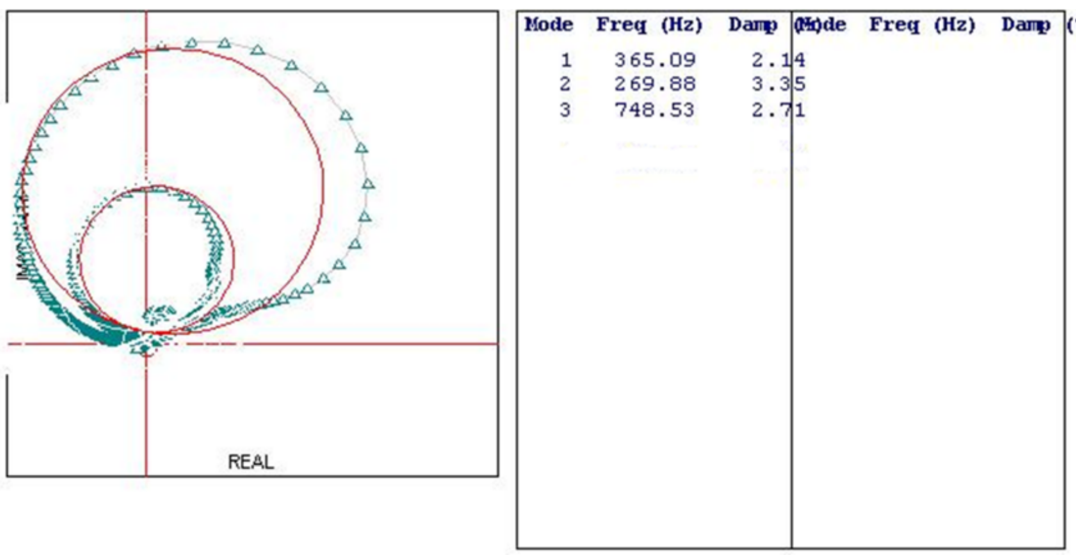

Figure 4.51 – Modes Shapes identified for Frame 3 loaded Up to 500 N

It were only identified the three known mode shapes.

For the load level of *3500 N*, whose FRF is presented in Figure 4.52, it were identified two new mode shapes.

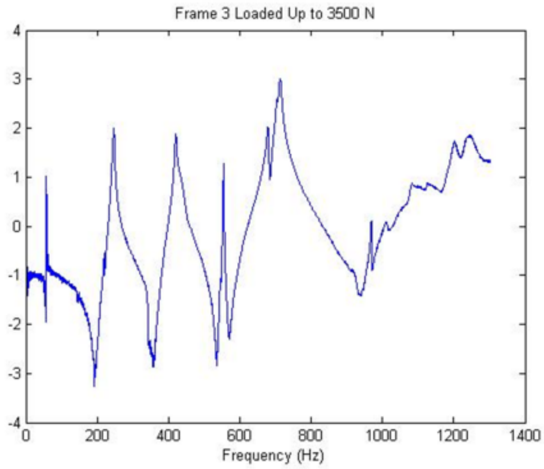

Figure 4.52 – FRF from Frame 3 Loaded Up to 3500 N

The identification of the two new mode shapes is shown in Figure 4.53.

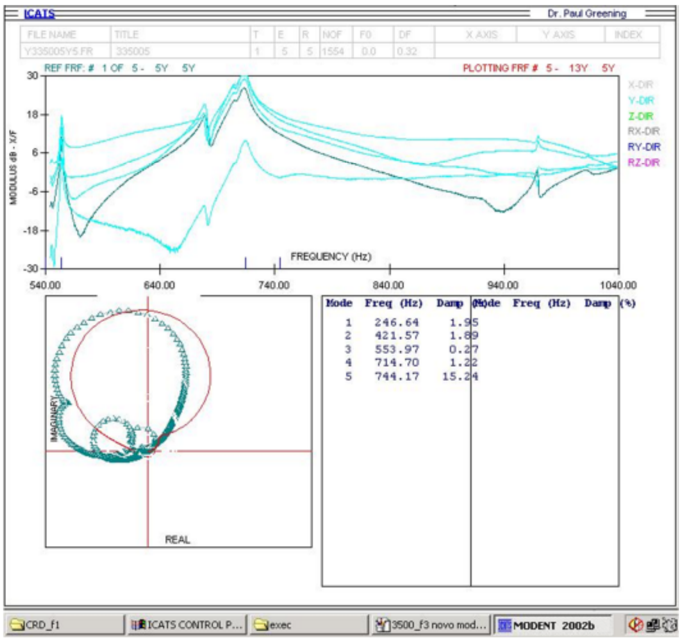

Figure 4.53 – Mode Shapes from Frame 3 identified in Icats

Although there were five mode shapes, the one with the natural frequency of 553,97 *Hz*, has disappear at the next load level where the mode shapes where studied – *4000 N.* This is a load level near failure and, by observing its FRF, it seems that it is emerging a new mode shape from the third one, which is already known and whose frequency is the natural frequency *2.* All mode shapes related to this load level are presented in Figure 4.54.

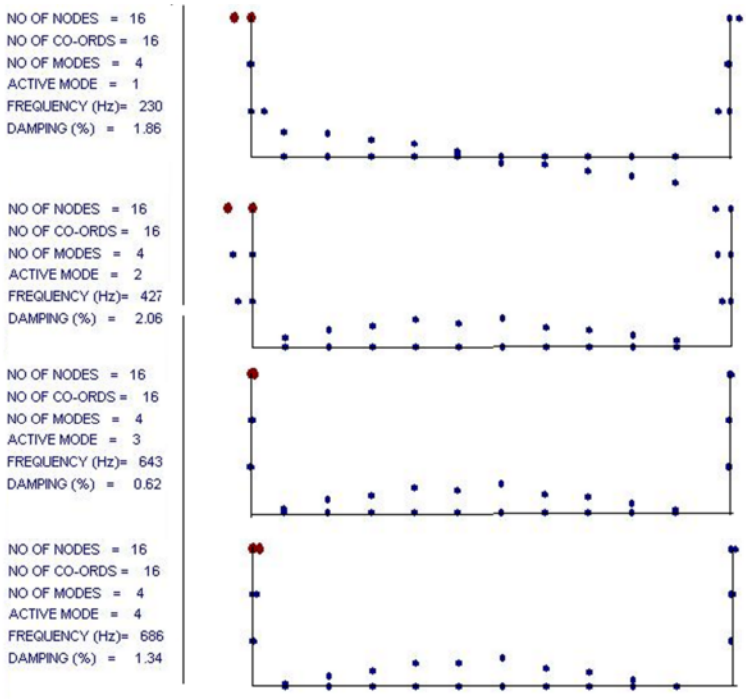

Figure 4.54 – Mode Shapes identified in Icats from Frame 3 at a Load Level of 4000 N

It should be noted that, as mentioned above, this new mode shape seems to have derived from the third one.

Both this new mode shapes the one corresponding to the natural frequency *1b* present, near failure, a very similar format to the mode shape whose natural frequency is the *2* – in this case mode shape 4.

Mode shape 1 seems that has kept the same format.

From the results shown above, with the emergence of a new mode shape that also seem to be emerging at the last level of loading on frame 1, it is suggested the test os another identical frame in order to confirm its existence or not.

5. Conclusions

In conclusion, it can be said that the main objectives of the project were achieved. Thus, were reached the optimal conditions to carry out study of the dynamic properties and were obtained the required results, showing enough consistency.

Thus, it will be addressed the main points to retain after this study.

First, it was performed the reinforced concrete structure where the dynamic tests took place, achieving data collection while it was experiencing compression and flexion. In addition, it was developed a mechanism that has allowed in, a simple way, the variation of load applied to the structure. With this, was collected data since the frame was unloaded until load levels near failure.

Prior to dynamic tests, other tests that were carried out have allowed a better preparation of them and also a better understanding of the characteristics of the structure under study.

The modeling carried out in software *GSA* has provided the previous identification of the natural frequencies to study on the dynamic tests. It should be mentioned that it has proven to be effective on the modeling of the structure without the steel bar, but not so much when the modeling with the bar. In fact, the experimental results have shown higher values for the natural frequencies; more than the double of those from the numerical program.

Regarding to dynamic tests, it was verified a decrease around 2% of the first three natural frequencies of the structure unloaded in just nine days. This test was initiated 28 days after casting.

In the study of the variation of the modal properties with increasing the static load, were initially identified two mode shapes, in the sample rate under study. However, when the load was applied, it was developed a new mode from the first. It was found the increase of the separation between these two modes, which initially were just one, with the increase of the static load. That happened with the reduction of the natural frequency *1a* and with the increase of the natural frequency *1b.* It was found a reduction for the natural frequency *2,* although it decreased more smoothly.

The consistency of data was supported by the test of two identical frames, which have shown the same trend for each one of the three natural frequencies. Thus, it was verified a decrease on natural frequency *1a* of 10% for both frames, an increase of 35% for frame 1 and 58% for frame 3 on natural frequency *1b* and finally a reduction of 5% in frame 1 and 8% in frame 3 on natural frequency *2.*

It was found some differences between the two frames. The initial application of the static load was more influent in changing natural frequencies in frame 3, while in the frame 1 was verified that changes were more significant in the initial loads, but after the load was applied.

It was demonstrated that the approach of failure and therefore the increase of deterioration of the structure led to the emergence of one or more mode shapes, particularly in the frame 3, whose FRF's have shown several peaks in higher load levels. This frame has behaved very sensitive by presenting in some load cycles great changes on its FRF's both to the level of natural frequencies value and also at the emergence of new mode shapes. However, it was also verified the imminent appearance of a new mode shape for higher load levels on FRF's of frame 1, which seemed to derivate from the last mode shape under study.

It was used the software *Icats* in an attempt to identify new mode shapes, which has happened in some load levels. It were also reproduced the identified mode shapes at some load levels and it was verified that the second mode shape – natural frequency *1b*– has similar format to the third mode shape instead to the first, from which it has emerged. It was not found any evident change on the format of these three modes with the increasing of load.

It is worth to mention that the dynamic analysis carried out in the direction perpendicular, although not perfectly effective in helping to understand some questions, can be an efficient test in some situations.

Regarding the study of damping, this was the test with less satisfactory results, not reaching a correlation with the variation of static load. It seemed that natural frequencies have changed in a different way among them. However, here too the results were consistent in both frames tested.

As further work, it could be tested another identical frame in order to try to achieve a better understanding about some data obtained in frame 3.

It was found that, for some load levels, there were some sudden changes on dynamic characteristics so it may be tested another frame with lower load cycles.

In order to achieve a greater consistency of the obtained results, another frame could be tested with cycles of loading/unloading.

Dynamic analysis can be made in *GSA* model, for the load cycles experienced, and compare the results with those obtained experimentally.

In addition, this may have been one more step to achieve a greater harmony between the results obtained by experimental tests and those obtained in numerical programs.

References

ADAMS, R. D. et al (1978). "A vibration technique for non-destructively assessing the integrity of structures" *J. Mechanical Engineering* Science, 20(2), 93-100

BAPTISTA, M. A. Et al (2004). "Análise Experimental para Obtenção das Características Dinâmicas do Edifício da Portugal Telecom no Parque das Nações."

BRUN, M.: REYNOUARD, J. M. and JEZEQUEL, L. (2003). "A simple shear wall model taking into account stiffness degradation." *J. Engineering Structures*. 25(1). 1-9

BROWNJOHN, J. M.W.; DUMANOGLU, A. A. (1994) "Dynamic investigation of a suspension footbridge." *J. Engineering Structures*, 16(6), 395-406

CAWLEY, P.; ADAMS, R. D. (1979). "The location of defects in structures from measurements of natural frequencies." *J. Strain Analysis*, 14(2) 49-52

CHOPRA, A. K. (1995). "Dynamic oF Structures: Theory and Applications to Earthquake Engineering." Prentice Hall, New Jersey

CLOUGH, R.; PENZIEN J. (1993). "Dynamic of Structures: 2nd Edition." McGraw-Hill, New-York.

CHEN, H. L.; SPYRAKOS, C. C. and VENKATESH, G. (1995). "Evaluating structural deterioration by dynamic response." *J. Structural Engineerin*g, 121(8), 1197-1204

EWINS, D. (2000). "Modal Testing: Theory, Practice and Application: 2nd Edition." Research Studies Press

EUROCODE 2 (2004) "EN 1992-1-1: Eurocode 2: Design of concrete structures – Part 1-1: General rules and rules for buildings", CEN, Brussels, Belgium, 2004

HORNE, M. (2009). "Detailed Dynamic Modeling of a Loaded Reinforced Concrete Frame."

MEIRELES, J. F. B. (2007). "Análise Dinâmica de Estruturas por Modelos de Elementos Finitos Identificados Experimentalmente"

MENDES, P.; OLIVEIRA, S., (2008). "Análise Dinâmica de Estruturas – Utilização Integrada de Modelos de Identificação Modal e Modelos de Elementos Finitos"

NÓBREGA, P. G. B.; HANAI, J. B. (2005). "The modal analysis on the evaluation of concrete precast structures."

TIAN, M. G.; YI, W.J. (2008) "Dynamic Behavior of reinforced concrete frame during construction." *J. Central South University of Technology*. 15(3). 418-422.

ZEMBATY, Z.; KOWALSKI, M.; POSPISIL, S. (2006). "Dynamic identification of a reinforced concrete frame in progressive states of damage." *J. Engineering Structures*. 28(5). 668-681

APPENDICES

1. Reinforcement Steel Test

The steel bar strength is given by the follow expression.

$$f_y(MPa) = \frac{F(N)}{A(mm^2)}$$

were,

$$A = \frac{\pi\phi^2}{4}$$

Three steel bars were tested until failure. Both maximum load and diameters of the two parts of the broken steel bar were measured. Results are presented in the table 1.

Table 1

Bar	F (KN)	ϕ_1 (mm)	ϕ_2 (mm)	ϕ (mm)	A (mm^2)	f_y (MPa)
1	13	6,62	6,68	6,65	34,73	374,29
2	13	6,58	6,68	6,63	34,52	376,55
3	13	6,72	6,56	6,64	34,73	375,42

By averaging,

$$f_y = 375{,}42\ MPa$$

2. Maximum Horizontal Displacement

Next figures show the determination of the maximum displacements on the frame, which correspond to a *4,5 KN* load. It was used the software *Ftoll* in order to determine those displacements. It must be noted that this software does not allow the condition *free* for supporting, so the frame was modeled as it is represented in Figure 1 After all the sections, materials and supports were introduced, the model of the frame was determined and it is represented on the next figure.

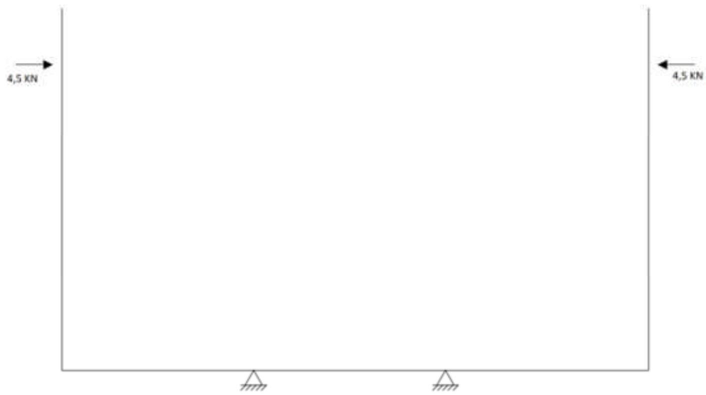

Figure 1

Using the referred software, it was determined the maximum horizontal displacement, which is represented in Figure 2.

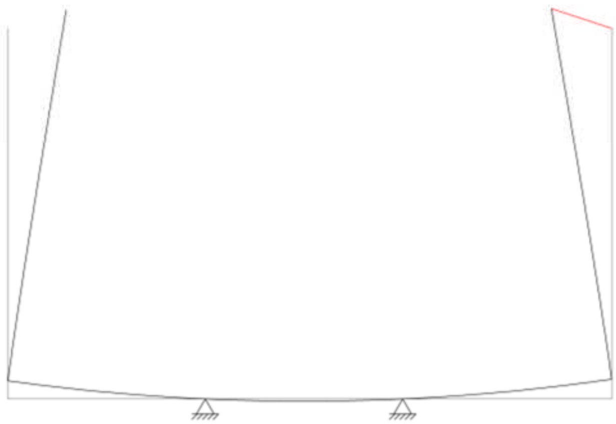

Figure 2

That maximum horizontal displacement is:

$$d_x = 2{,}3\ mm$$

3. Beam Test

The beam presented in figures 3.21 to 3.23 was tested until failure in concrete laboratory in order to determine its ultimate moment. In figure 3 is presented a scheme of the test.

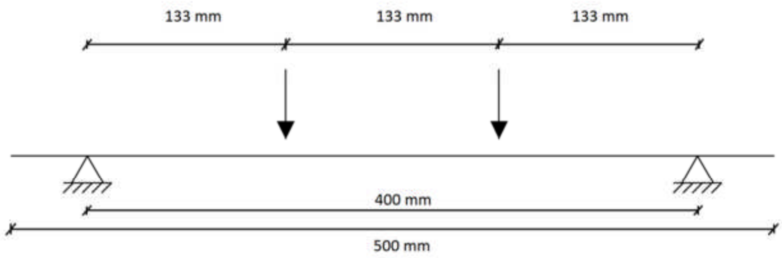

Figure 3 – Scheme of the Test

This test was made on a machine which applies a single load that is then transmitted to two metal plates, represented in figure 3 by the arrows.

The maximum load registered was the follow:

$$F_{max} = 18{,}2\ KN$$

That means that it were applied two similar loads on the beam with the value of *9,1 KN.*

In figure 4 is represented the bending moment diagram of the beam.

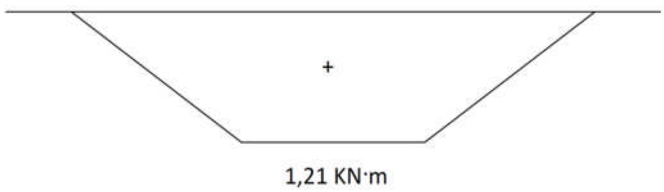

Figure 4 – Bending Moment Diagram

So the ultimate moment of this beam is:

$$M = 1{,}21\ KN \cdot m$$

4. Compressive Strength of Concrete

This test consisted of compressing the concrete cubes until failure, measuring the maximum load. Knowing that value and knowing the cubes section, the compressive strength of concrete can be determined by the following expression

$$\sigma_c = \frac{F}{A}$$

The cubes have a $0{,}05 \times 0{,}05\ m^2$ section.

Data referred to this test is presented in Table 2.

Table 2

F (KN)	*A (m^{2})*	σ_c *(KPa)*
91,1	0,0025	36440
84,3	0,0025	33720
82,8	0,0025	33120

By making an average of the last column values, the compressive strength of concrete is the follow:

$$\sigma_c = 34{,}4\ MPa$$

5. Load Cell Calibration

In tables 3, 4 and 5 are presented the results of the load cell calibration test. It should be mentioned that:

$$1\ Kg = 9{,}81\ KN$$

Table 3

Weight (Kg)	*Load (N)*	*Strain*
0	0	0,00
1	9,81	0,03
2	19,61	0,06
3	29,42	0,09
4	39,23	0,12
5	49,03	0,15
6	58,84	0,18
7	68,65	0,21
8	78,45	0,24
9	88,26	0,27
10	98,07	0,3
11	107,87	0,33
12	117,68	0,36
13	127,49	0,39
14	137,29	0,42
15	147,10	0,45
16	156,91	0,48
17	166,71	0,51
18	176,52	0,54
19	186,33	0,57
20	196,13	0,6

Table 4

Weight (Kg)	*Load (N)*	*Strain*
0	0,00	0,00
2	19,61	0,06
4	39,23	0,12
6	58,84	0,18
8	68,65	0,24
10	88,26	0,3
12	117,68	0,36
14	137,29	0,42
16	156,91	0,48
18	176,52	0,54
20	196,13	0,6

Table 5

Weight (Kg)	*Load (N)*	*Strain*
0	0	0,00
5	49,03	0,15
10	98,07	0,3
15	147,10	0,45
20	196,13	0,6

Figure 4 shows the *Load vs Strain* graphic.

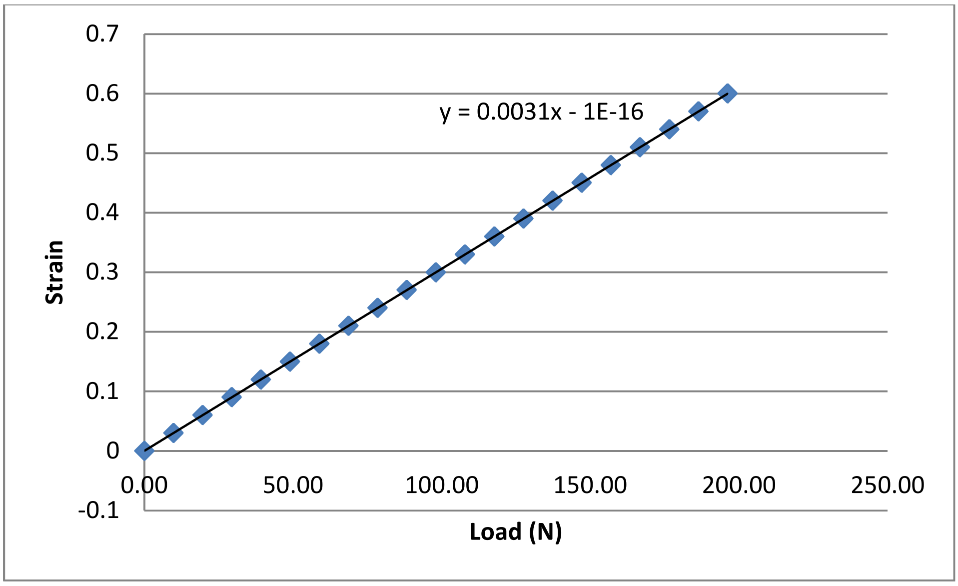

Figure 5

6. Frequency *vs* Load

Load (N) *Frame 1* *Frame 3*

0

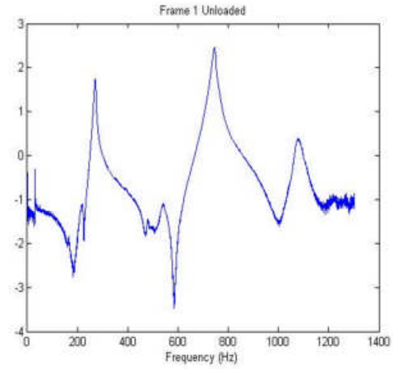

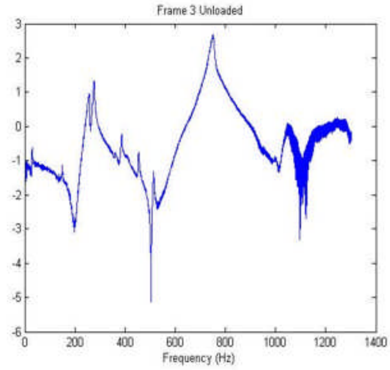

125

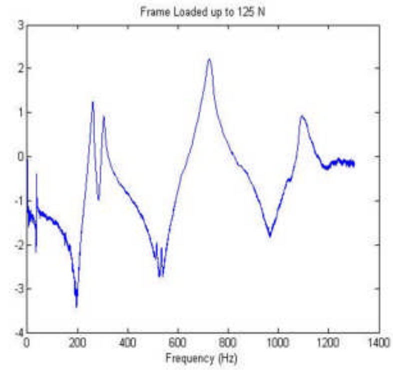

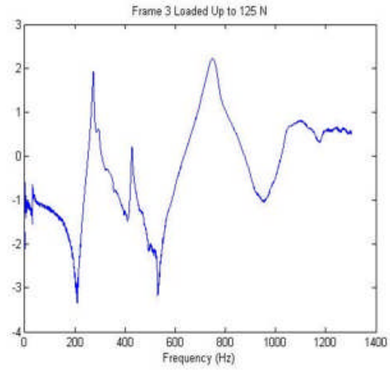

250

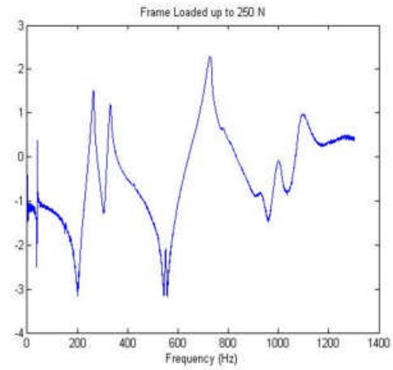

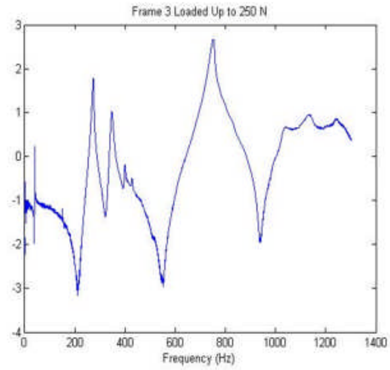

375

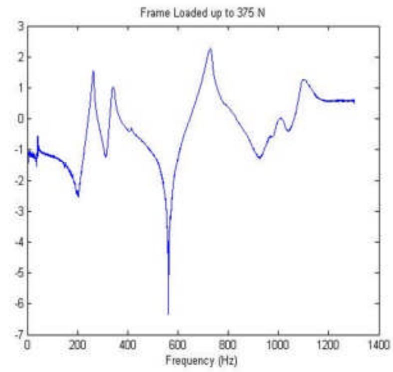

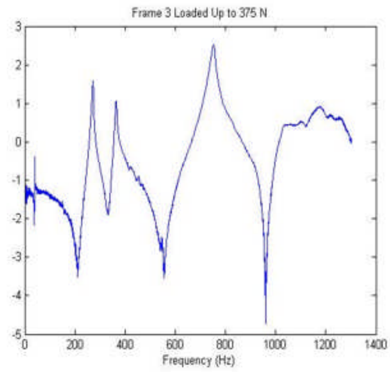

500

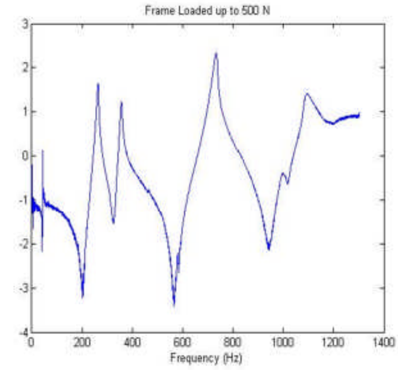

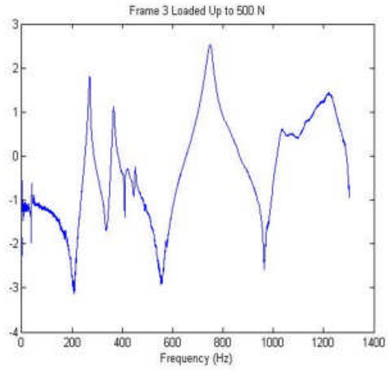

625

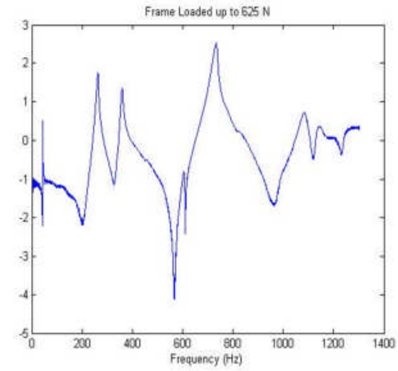

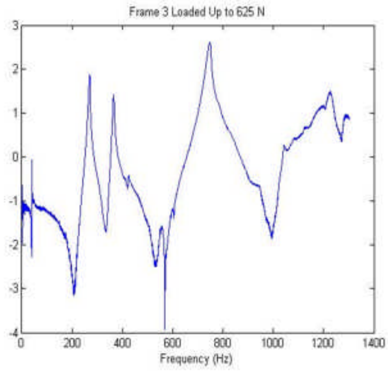

750

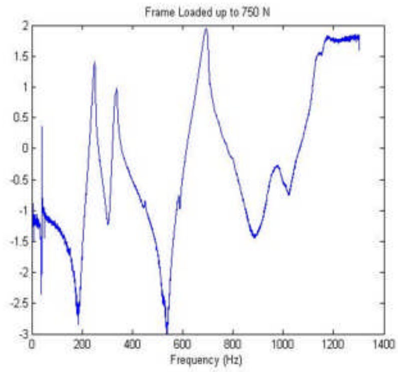

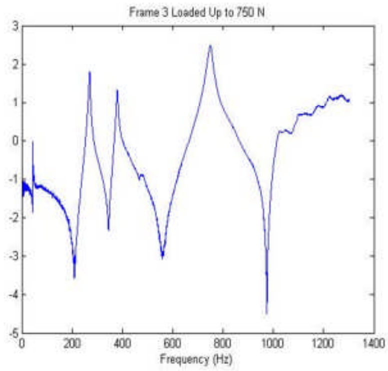

875

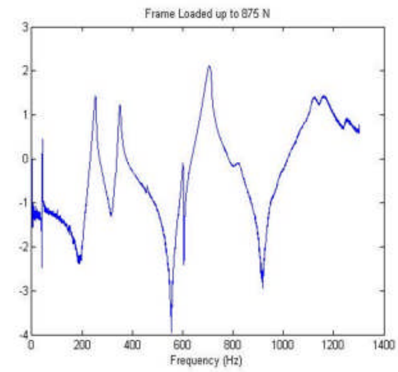

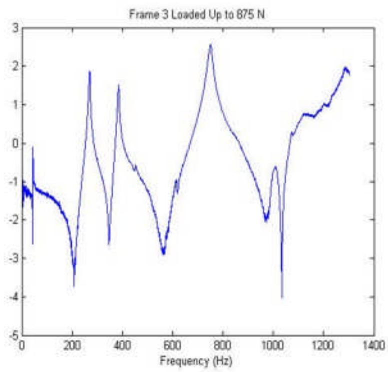

1000

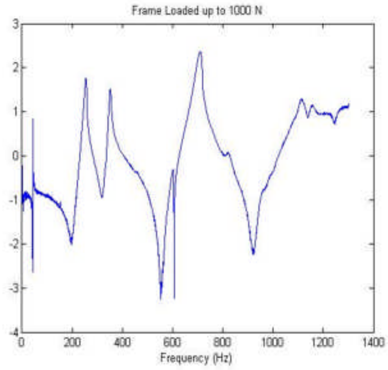

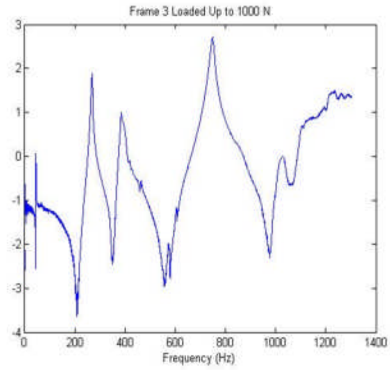

1125

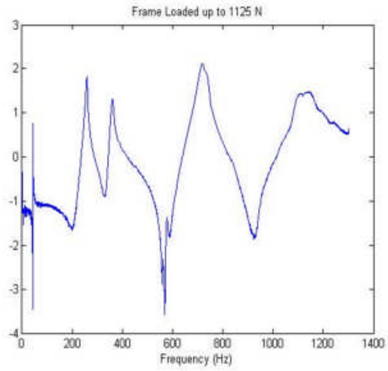

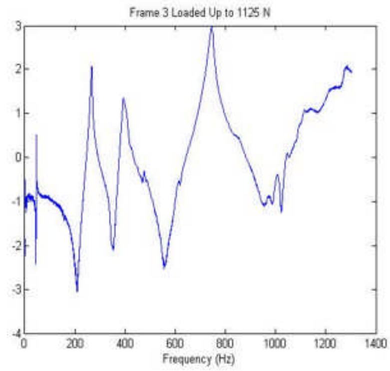

1250

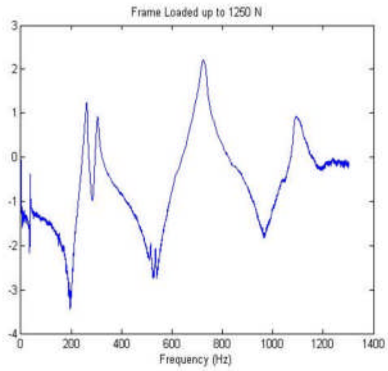

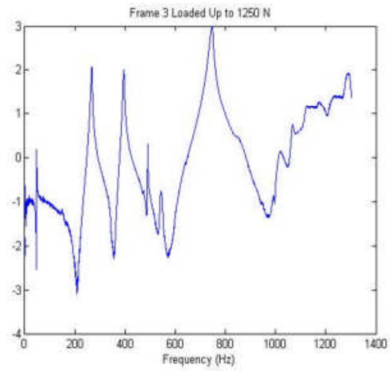

1375

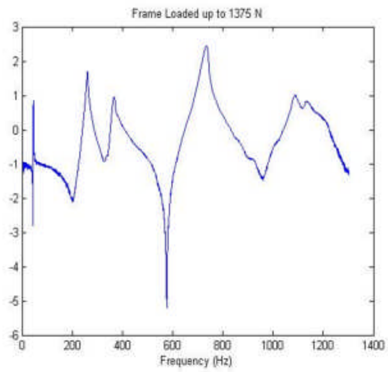

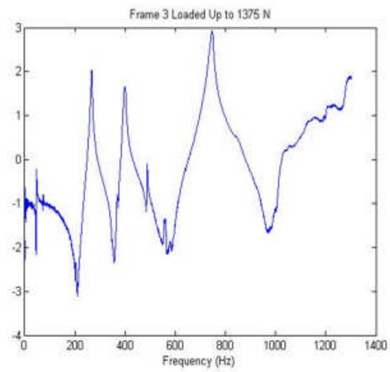

1500

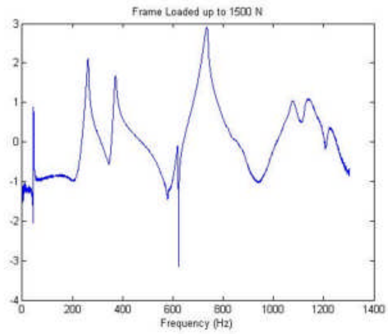

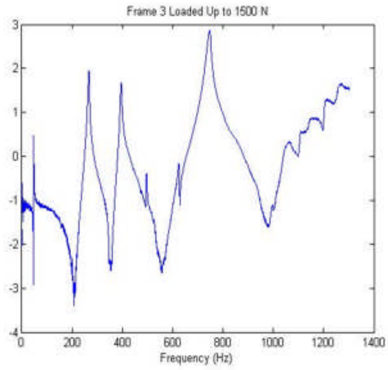

1625

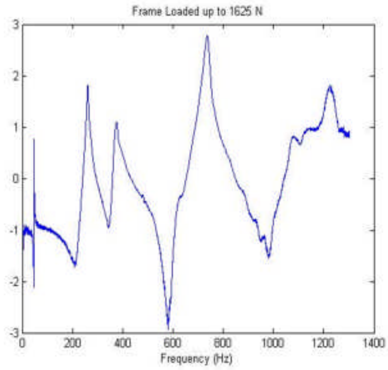

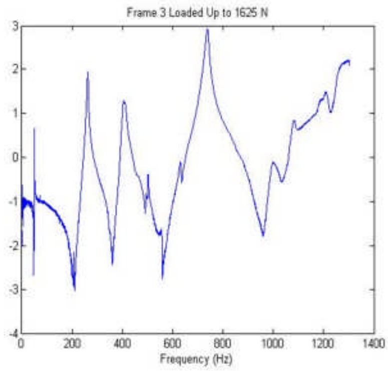

1750

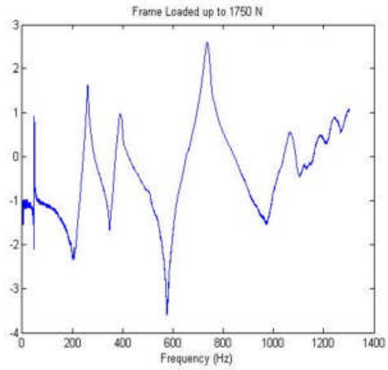

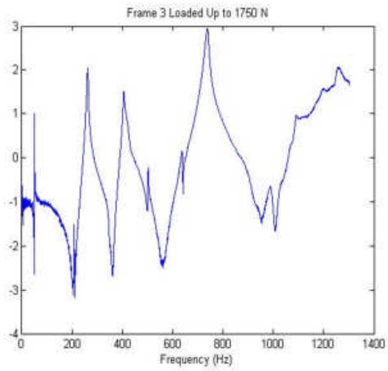

1875

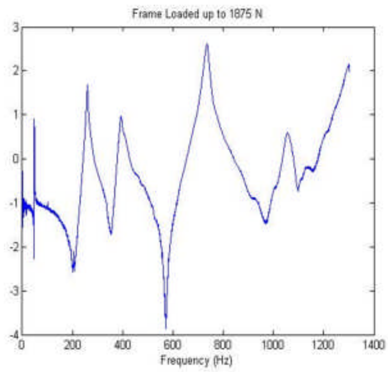

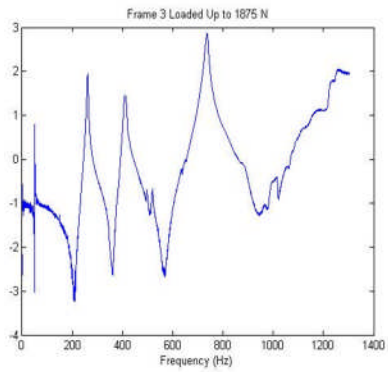

2000

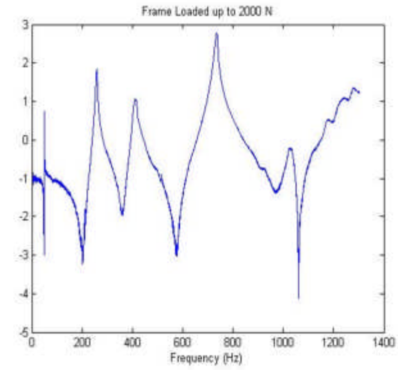

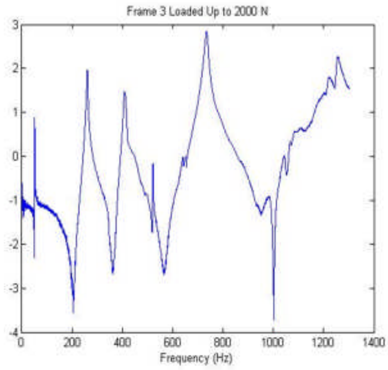

2125

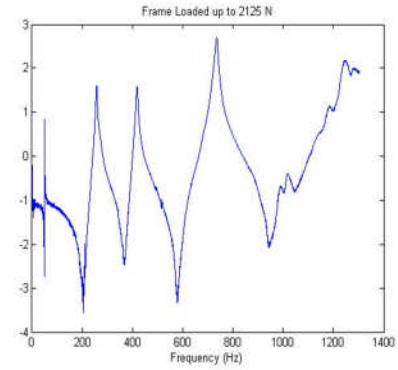

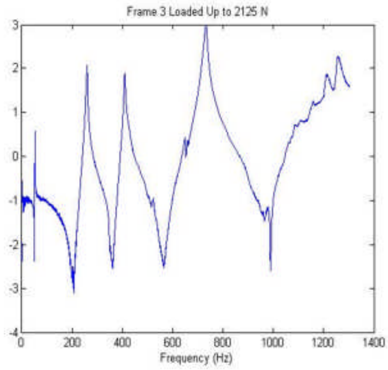

2250

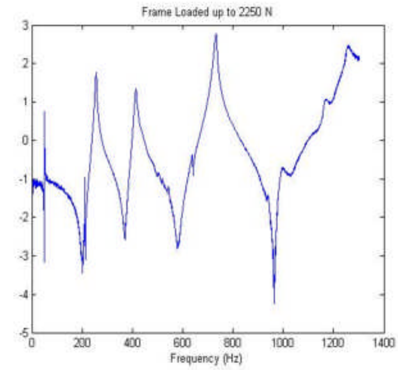

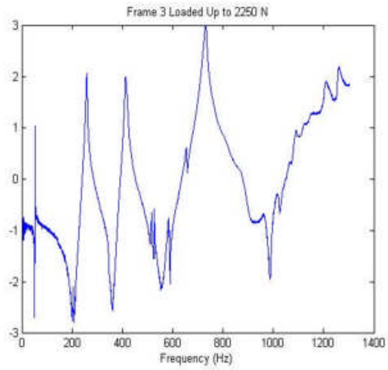

2375

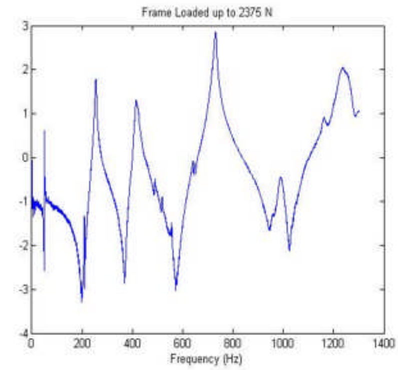

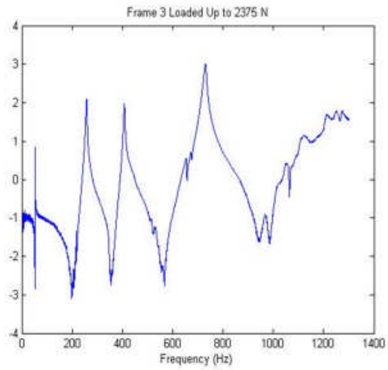

2500

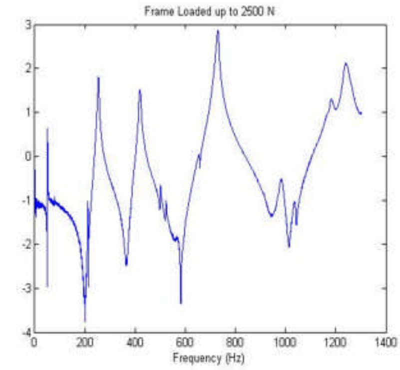

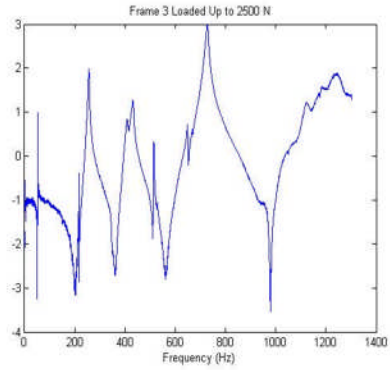

2625

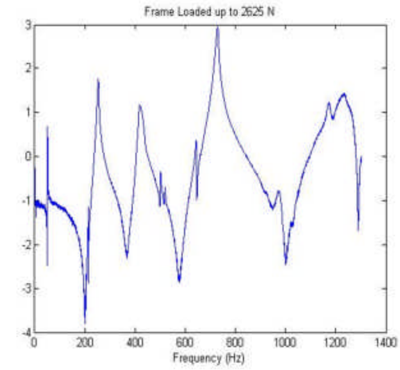

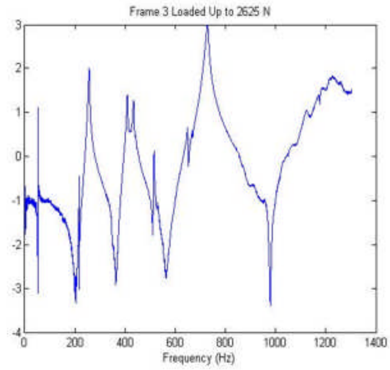

2750

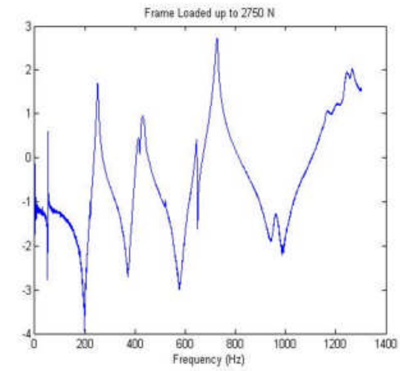

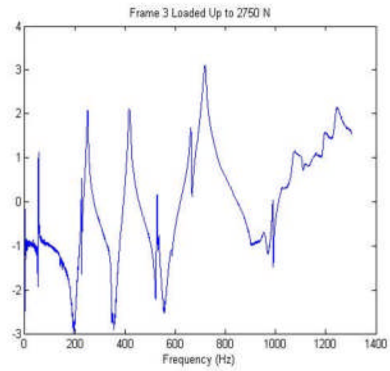

2875

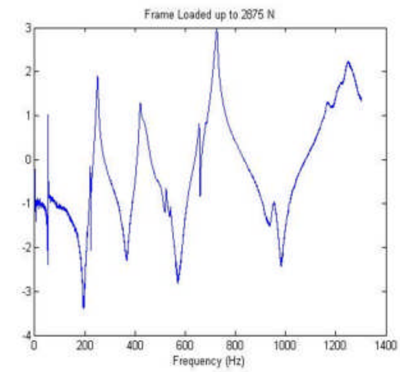

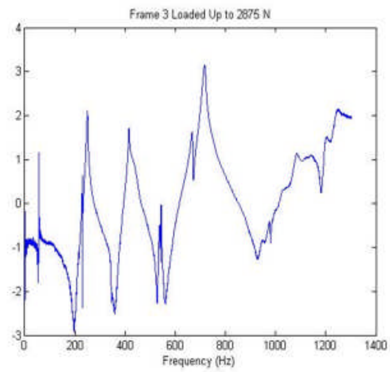

3000

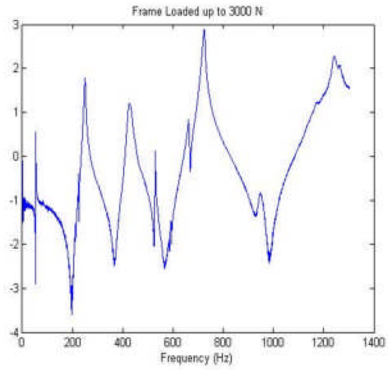

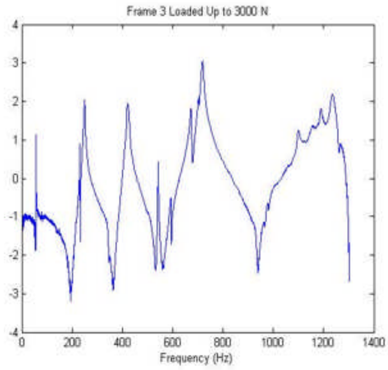

3125

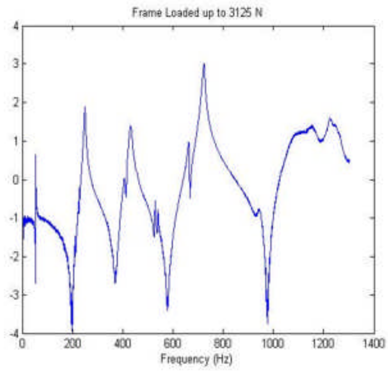

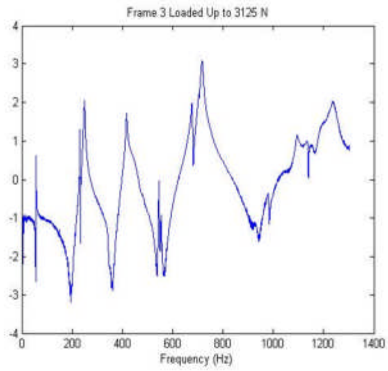

3250

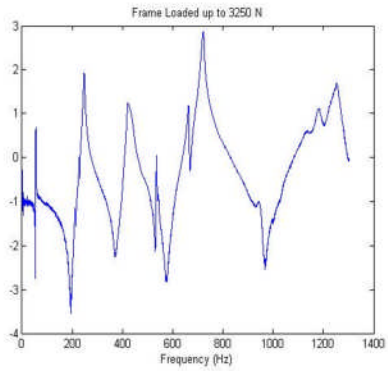

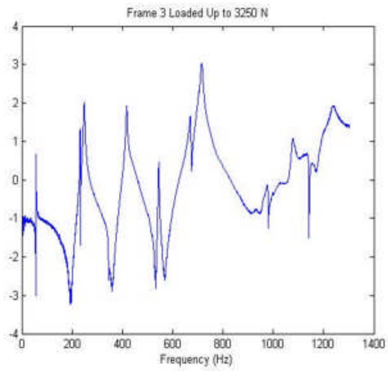

3375

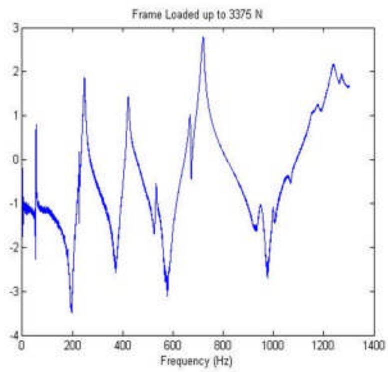

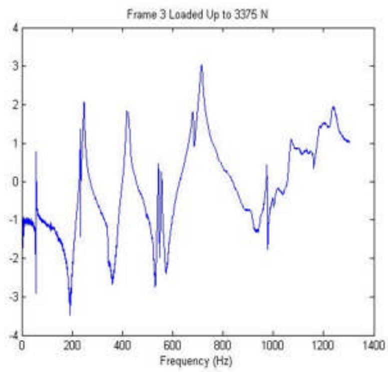

3500

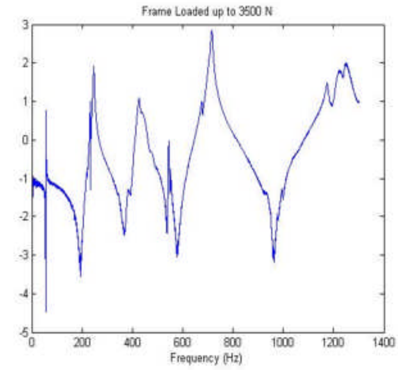

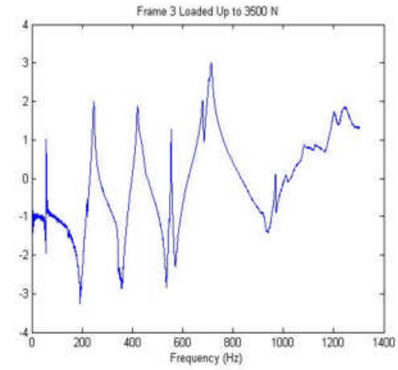

3625

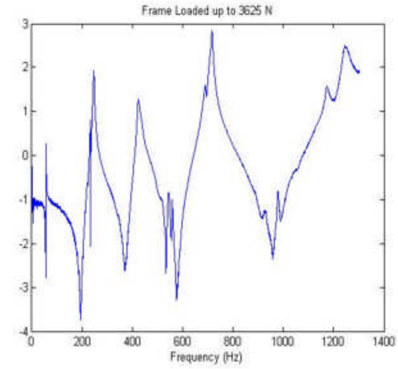

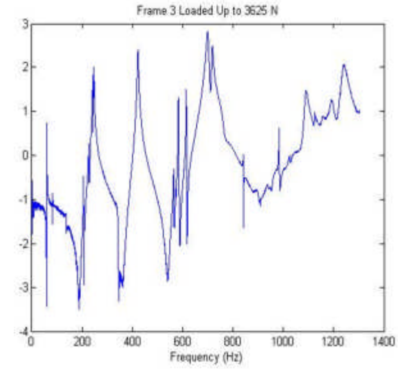

3750

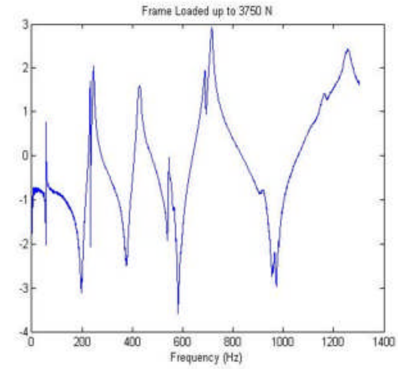

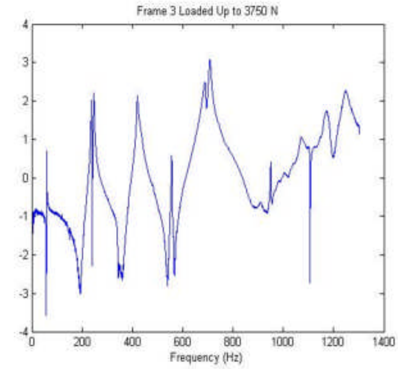

3875

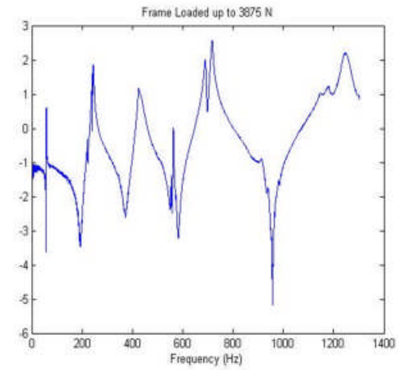

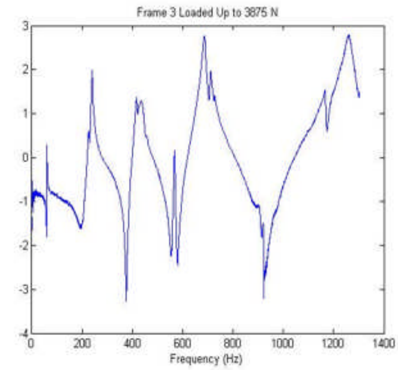

4000

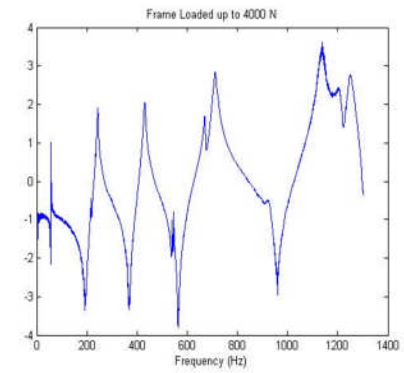
Frame Loaded up to 4000 N
Frequency (Hz)

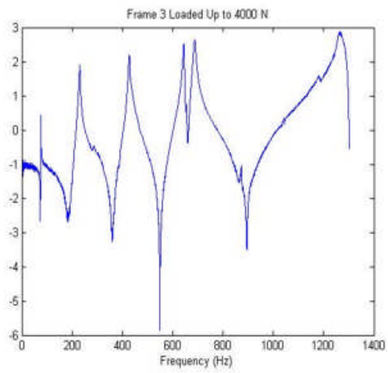
Frame 3 Loaded Up to 4000 N
Frequency (Hz)

7. Damping vs Load

	Damping (%)					
Load	*Frame 1*			*Frame 3*		
(%)	*Mode 1a*	*Mode 1b*	*Mode 2*	*Mode 1a*	*Mode 1b*	*Mode 2*
0	-	2,39	1,67	1,97	1,68	2,23
125	2,33	3,81	1,17	1,71	0,78	5,17
250	2,78	2,97	2,87	1,79	2,82	2,22
375	2,88	4,07	2,42	1,98	1,98	1,67
500	2,71	2,44	2,13	3,35	2,14	2,71
625	2,57	1,32	1,97	1,98	1,80	1,85
750	3,67	3,02	3,33	1,79	1,65	1,99
875	3,18	2,64	2,42	1,92	1,55	1,98
1000	4,17	2,99	2,97	1,82	1,98	1,85
1125	2,92	2,34	1,13	1,26	0,83	1,94
1250	N/A	N/A	N/A	1,27	0,71	1,71
1375	2,72	3,92	2,82	0,98	0,61	1,57
1500	2,78	2,42	2,04	1,88	1,48	1,73
1625	2,40	2,67	2,12	1,84	2,57	1,66
1750	2,39	5,78	0,57	1,97	1,32	1,61
1875	2,40	3,08	1,86	1,84	3,30	1,69
2000	2,15	4,12	1,53	2,20	1,98	1,56
2125	2,38	1,83	1,50	1,92	1,29	1,71
2250	2,28	2,28	1,44	1,86	2,01	1,85
2375	1,79	2,36	1,08	1,80	1,26	1,58
2500	2,00	2,48	1,88	1,66	2,41	1,50
2625	2,19	4,70	1,37	1,90	1,19	1,51
2750	2,26	3,71	1,44	2,14	2,51	1,50
2875	2,25	1,86	1,43	2,02	1,29	1,37
3000	2,18	4,63	1,33	1,77	2,63	1,30
3125	2,09	3,31	1,29	1,84	1,21	1,29
3250	2,12	2,60	1,42	1,68	1,13	1,26
3375	1,46	1,57	1,06	1,29	1,23	1,15
3500	2,54	2,64	1,51	1,95	1,89	-
3625	1,88	2,93	1,22	1,19	1,06	1,29
3750	1,88	1,63	1,29	1,29	1,23	1,19
3875	1,60	2,44	1,07	1,88	1,71	1,57
4000	1,72	1,75	1,93	1,86	2,06	-